Article

Immunity

Cell Survival and Cytokine Release after Inflammasome Activation Is Regulated by the Toll-IL-1R Protein SARM

Graphical Abstract

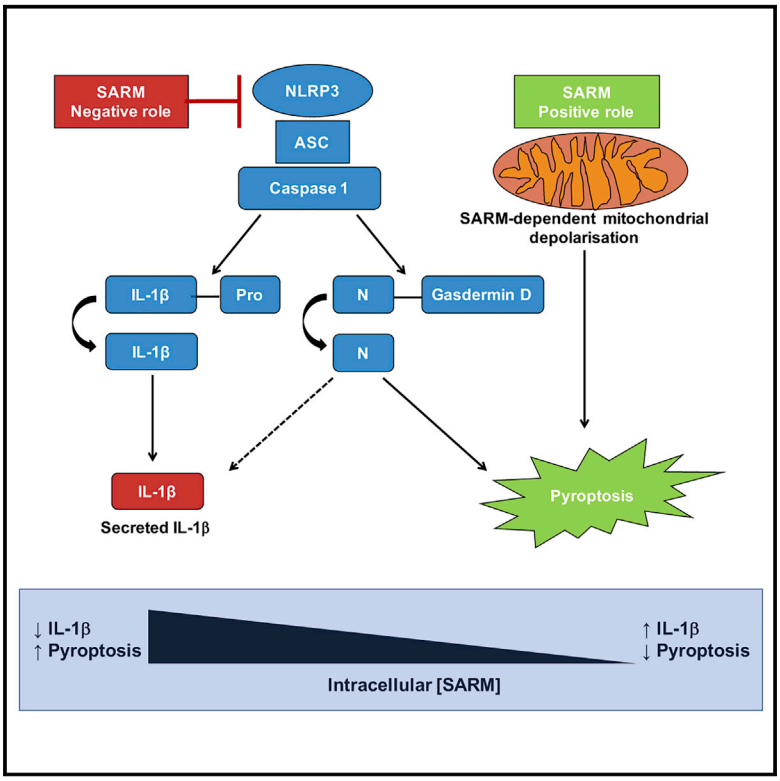

Highlights

- NLRP3 inflammasomes stimulate IL-1β release either with or without cell death
- The TIR protein SARM negatively regulates NLRP3 to reduce IL-1β release
- SARM-mediated mitochondrial depolarization (MDP) is required for optimal pyroptosis
- NLRP3 activators that don't kill cells fail to cause SARM-dependent MDP

Authors

Michael Carty, Jay Kearney, Katharine A. Shanahan, ..., Ed C. Lavelle, Padraic G. Fallon, Andrew G. Bowie

Correspondence

agbowie@tcd.ie

In Brief

NLRP3 inflammasome activation causes IL-1β release either with or without cell death, but how cells regulate these outcomes is unclear. Carty et al. show that the TIR protein SARM negatively regulates IL-1β release by directly targeting NLRP3 yet is required for maximal pyroptosis by facilitating mitochondrial depolarization.

Carty et al., 2019, Immunity *50*, 1412–1424
June 18, 2019
https://doi.org/10.1016/j.immuni.2019.04.005

CellPress

CellPress

Immunity
Article

Cell Survival and Cytokine Release after Inflammasome Activation Is Regulated by the Toll-IL-1R Protein SARM

Michael Carty,[1,4] Jay Kearney,[1,4] Katharine A. Shanahan,[1] Emily Hams,[2] Ryoichi Sugisawa,[1] Dympna Connolly,[1] Ciara G. Doran,[1] Natalia Muñoz-Wolf,[1] Claudia Gürtler,[1] Katherine A. Fitzgerald,[3] Ed C. Lavelle,[1] Padraic G. Fallon,[2] and Andrew G. Bowie[1,5,*]

[1]School of Biochemistry and Immunology, Trinity Biomedical Sciences Institute, Trinity College Dublin, Dublin 2, Ireland
[2]School of Medicine, Trinity Biomedical Sciences Institute, Trinity College Dublin, Dublin 2, Ireland
[3]Division of Infectious Diseases and Immunology, University of Massachusetts Medical School, Worcester, MA, USA
[4]These authors contributed equally
[5]Lead Contact
*Correspondence: agbowie@tcd.ie
https://doi.org/10.1016/j.immuni.2019.04.005

SUMMARY

Assembly of inflammasomes after infection or injury leads to the release of interleukin-1β (IL-1β) and to pyroptosis. After inflammasome activation, cells either pyroptose or enter a hyperactivated state defined by IL-1β secretion without cell death, but what controls these different outcomes is unknown. Here, we show that removal of the Toll-IL-1R protein SARM from macrophages uncouples inflammasome-dependent cytokine release and pyroptosis, whereby cells displayed increased IL-1β production but reduced pyroptosis. Correspondingly, increasing SARM in cells caused less IL-1β release and more pyroptosis. SARM suppressed IL-1β by directly restraining the NLRP3 inflammasome and, hence, caspase-1 activation. Consistent with a role for SARM in pyroptosis, *Sarm1*$^{-/-}$ mice were protected from lipopolysaccharide (LPS)-stimulated sepsis. Pyroptosis-inducing, but not hyperactivating, NLRP3 stimulants caused SARM-dependent mitochondrial depolarization. Thus, SARM-dependent mitochondrial depolarization distinguishes NLRP3 activators that cause pyroptosis from those that do not, and SARM modulation represents a cell-intrinsic mechanism to regulate cell fate after inflammasome activation.

INTRODUCTION

Inflammasomes detect pathogens and host-derived danger signals, leading to activation of the inflammatory caspases caspase-1 and caspase-11. These caspases regulate cytokine release and cell death, which can contribute to pathogen clearance and restoration of homeostasis or can exacerbate tissue damage, leading to chronic inflammation (Broz and Dixit, 2016). The best characterized inflammasome assembles in response to activation of NLR family pyrin domain containing 3 (NLRP3), a component protein of an inflammasome that senses a range of diverse pathogens and cellular insults. NLRP3 contains a pyrin domain (PYD), and after activation, it undergoes PYD-dependent oligomerization, leading to recruitment and nucleation of the adaptor protein ASC, which contains both a PYD and a caspase activation and recruitment domain (CARD). Such ASC oligomerization enables the ASC CARDs to recruit and cluster pro-caspase-1, leading to its processing to active caspase-1 (Broz and Dixit, 2016).

Two major functional outcomes of caspase-1 activation in macrophages are the processing of pro-interleukin-1β (pro-IL-1β), leading to release of active IL-1β, and caspase-1-dependent inflammatory cell death, termed pyroptosis (Broz and Dixit, 2016). Intracellular lipopolysaccharide (LPS) from bacteria can also activate a non-canonical inflammasome pathway that involves caspase-11-mediated pyroptosis and NLRP3-dependent IL-1β production (Broz and Dixit, 2016). Recently, gasdermin D (GSDMD) has been shown to be a substrate for both caspase-1 and caspase-11, and GSDMD cleavage generates an N-terminal fragment, leading to the generation of plasma membrane pores. (He et al., 2015; Kayagaki et al., 2015; Shi et al., 2015). Pore formation by GSDMD was initially proposed to be both necessary and sufficient for pyroptosis and to concomitantly facilitate IL-1 release (Aglietti et al., 2016; Ding et al., 2016; Liu et al., 2016; Sborgi et al., 2016). However, this concept does not take account of studies published both before and since the discovery of GSDMD pores, which demonstrate inflammasome activation leading to IL-1 release in the absence of pyroptosis (Chen et al., 2014; Conos et al., 2016; Evavold et al., 2018; Gaidt et al., 2016; Heilig et al., 2018; Wolf et al., 2016; Zanoni et al., 2016). It is now appreciated that GSDMD pores can facilitate IL-1β release from non-pyroptosing living cells after NLRP3 inflammasome activation (Evavold et al., 2018; Heilig et al., 2018) and that GSDMD-independent mechanisms of IL-1β release also exist (Monteleone et al., 2018). GSDMD pores are now thought of as necessary, but not sufficient, for the osmotic collapse of cells that leads to pyroptosis, and further, the pores themselves can be regulated by membrane repair mechanisms (Rühl et al., 2018). Thus, cell-intrinsic mechanisms to regulate cell fate after inflammasome activation—which would define, for example,

why so-called hyperactivating ligands cause NLRP3-dependent IL-1β release without pyroptosis (Evavold et al., 2018; Zanoni et al., 2016)—remain to be defined.

Apart from macrophages, other terminally differentiated cell types can undergo regulated cell death in response to pathogens or host damage. One ancient innate immune protein that has recently been shown to have a role in mammalian neuronal-cell death in response to infection and injury is SARM (Sterile α and HEAT Armadillo motif-containing protein), which contains a Toll-IL-1R (TIR) domain (O'Neill and Bowie, 2007). A TIR domain is normally predictive of a role in IL-1 or Toll-like receptor (TLR) signaling, and indeed, we previously have shown that SARM inhibits TIR-domain-containing adapter-inducing interferon-β (TRIF)-dependent TLR responses (Carty et al., 2006). However, SARM, which is the most conserved TIR-domain-containing protein, with orthologs in *C. elegans* (TIR-1), *Drosophila* (Ect4,) horseshoe crab (crSARM), and mammals (Carty and Bowie, 2019), also has TLR-independent roles. Thus, mammalian neuronal SARM is required for cell death following a variety of insults such as oxygen and glucose deprivation, nerve transection, and vincristine treatment (Gerdts et al., 2013; Kim et al., 2007; Osterloh et al., 2012). In the CNS, neuronal death during bunyavirus infection, restriction of West Nile virus, and the immune response to vesicular stomatitis virus are all SARM dependent (Hou et al., 2013; Mukherjee et al., 2013; Szretter et al., 2009). In the periphery, SARM contributes to apoptotic clearance of T cells after an immune response (Panneerselvam et al., 2013).

Because we previously established a role for SARM in macrophages and in regulating *Ccl5* gene induction (Gürtler et al., 2014) and because of the role of SARM in neuronal-cell death in response to pathogens, we considered whether SARM would regulate inflammasome-dependent cytokine release and cell death in macrophages. Here, we reveal a role for SARM in regulating cell fate after NLRP3 activation, in that SARM can negatively regulate NLRP3 to suppress IL-1 release but is required for optimal pyroptosis. Absence of SARM from macrophages uncouples cytokine release and pyroptosis upon inflammasome activation, whereby cells displayed increased IL-1β production but reduced pyroptosis, while increasing SARM protein in cells caused less IL-1β release and more pyroptosis. Further pyroptosis-inducing NLRP3 stimulants caused SARM clustering at the mitochondria and SARM-dependent mitochondrial depolarization (MDP), whereas hyperactivating NLRP3 stimulants did not. Thus, SARM-dependent MDP distinguishes NLRP3 activators that cause pyroptosis from those that do not. Hence, the amount of SARM protein expressed in cells and the ability of cell activators to mobilize SARM for MDP are factors that determine cell fate after inflammasome activation.

RESULTS

Absence of SARM Alters Cell Survival and Cytokine Release after NLRP3 Activation

Given the role of SARM in mediating neuronal-cell death and the fact that we previously found a role for SARM in regulation of chemokine induction in macrophages (Gürtler et al., 2014), we examined whether SARM would regulate cell death and cytokine production in the context of NLRP3 inflammasome activation. Thus, bone-marrow-derived macrophages (BMDMs) from wild-type (WT) and *Sarm1*$^{-/-}$ mice (Figure S1; Gürtler et al., 2014) were primed with either LPS or Pam_3CSK_4 before treatment with the commonly used NLRP3 activator nigericin. In both cases, pyroptosis, as measured by lactate dehydrogenase (LDH) release, was significantly inhibited in primary *Sarm1*$^{-/-}$ BMDMs compared to WT cells (Figures 1A and 1B). This was also true for immortalized BMDMs (iBMDMs) from WT versus *Sarm1*$^{-/-}$ mice (Figure S2A). The use of inhibitors of NLRP3 (MCC950) (Coll et al., 2015) and caspase-1 (YVAD) (Motani et al., 2011) confirmed that SARM-dependent cell death stimulated by treatment of cells with LPS and nigericin was indeed NLRP3 and caspase-1 dependent (Figure S2A).

Apart from pyroptosis, inflammasome activation in primed cells also leads to the production of mature IL-1β due to caspase-1-dependent processing of pro-IL-1β (Broz and Dixit, 2016). Further, in myeloid cells, inflammasome activation also leads to caspase-1-dependent IL-1α maturation and release (Gross et al., 2012). Because pyroptosis and IL-1 release are often intrinsically coupled, we expected that inflammasome-dependent IL-1 release would also be impaired in the absence of SARM. However, the opposite was true in that primary BMDMs lacking SARM showed significantly heightened release of IL-1β or IL-1α after NLRP3 inflammasome activation (Figures 1C and 1D). In contrast, tumor necrosis factor (TNF)-α release was comparable in WT and *Sarm1*$^{-/-}$ BMDMs (Figure 1E). Similar findings were also found in iBMDMs in terms of IL-1β and TNF-α release after NLRP3 inflammasome activation by nigericin (Figures S2B and S2C). Treatment of cells with MCC950 or YVAD confirmed that IL-1β release in both WT and *Sarm1*$^{-/-}$ iBMDMs was NLRP3 and caspase-1 dependent (Figure S2D), while these inhibitors did not affect TNF-α release (Figure S2E). Similar to primary BMDMs, IL-1α release was increased in the absence of SARM after NLRP3 activation in iBMDMs (Figure S2F). IL-18 production, a further consequence of NLRP3 activation (Guo et al., 2015), was also enhanced in iBMDMs lacking SARM (Figure S2G).

To confirm that the phenotype of *Sarm1*$^{-/-}$ cells was solely due to the absence of SARM protein in these cells, rescue experiments were performed by transient retroviral expression of Flag-SARM in *Sarm1*$^{-/-}$ iBMDMs (Figure 1F). After NLRP3 inflammasome activation in these cells, IL-1β production was reduced to a concentration similar to that seen for WT cells (Figure 1G), while LDH release was restored to an amount similar to that seen for WT cells (Figure 1H). These data show that SARM normally acts to reduce IL-1 production yet promote pyroptosis after NLRP3 inflammasome activation.

IL-1 Production and Pyroptosis Are Uncoupled in Cells Lacking SARM

The data thus far demonstrate that the removal of SARM from BMDMs has opposite effects on NLRP3-mediated pyroptosis and IL-1 release. This result was confirmed when the kinetics of pyroptosis and IL-1 release after NLRP3 activation were examined over a five-hour time course. *Sarm1*$^{-/-}$ BMDMs produced significantly more IL-1β (Figure 2A) and IL-1α (Figure 2B) but dramatically less LDH (Figure 2C) than WT cells. In order to determine whether this uncoupling occurred at the single-cell

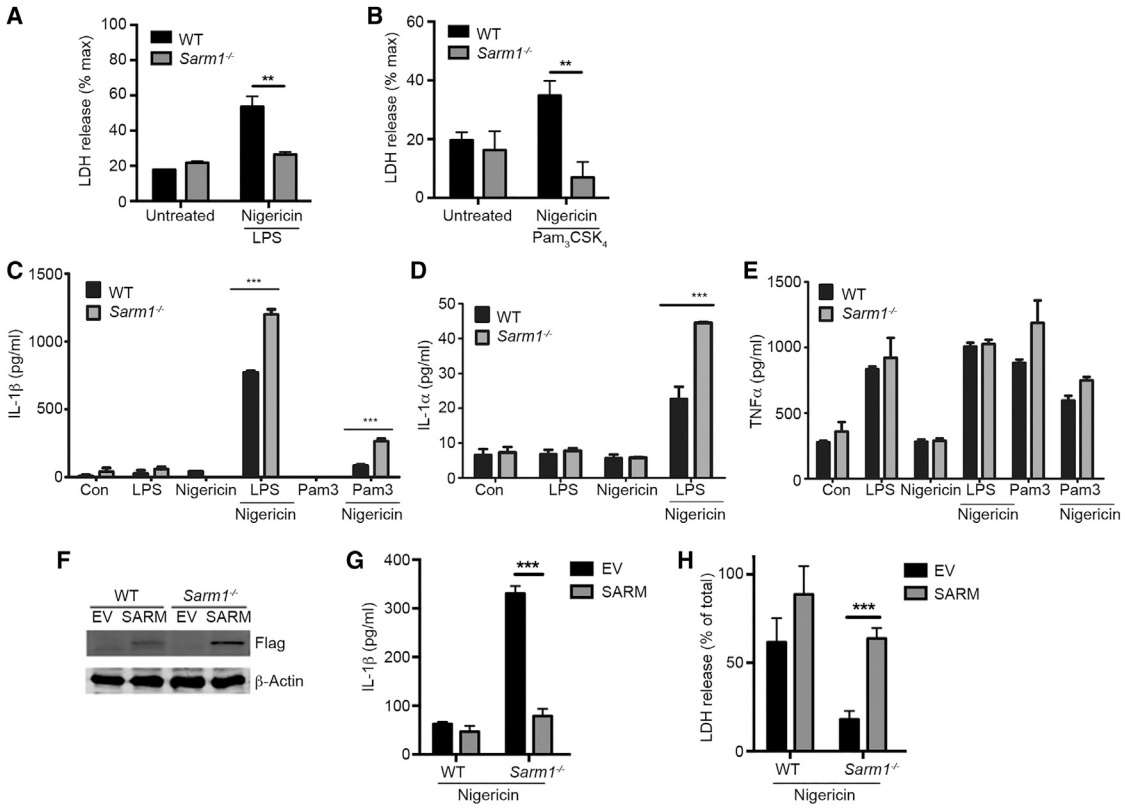

Figure 1. Opposing Role for SARM in Inflammasome-Stimulated Pyroptosis and IL-1 Production

(A and B) NLRP3 inflammasome-induced pyroptosis was triggered by treatment of WT and *Sarm1*$^{-/-}$ primary BMDMs primed with (A) LPS or (B) Pam_3CSK_4 by nigericin. Pyroptosis was assessed by LDH release.

(C–E) WT or *Sarm1*$^{-/-}$ primary BMDMs primed with LPS or Pam_3CSK_4 were treated with nigericin and IL-1β (C) IL-1α (D) or TNFα (E) were measured.

(F–H) Rescue of *Sarm1*$^{-/-}$ iBMDMs transiently expressing retrovirally expressed SARM. Cells primed with LPS were treated with nigericin and IL-1β (G) and pyroptosis (H) were measured. Immunoblot in (F) confirms retroviral expression of Flag-SARM in *Sarm1*$^{-/-}$ iBMDMs.

All data are mean ± SD of triplicate samples and are representative of three independent experiments. *$p < 0.05$, **$p < 0.01$, ***$p < 0.001$ (Student's t test). See also Figures S1 and S2.

level rather than being a cell-population phenomenon, iBMDMs were grown on anti-IL-1β-antibody-coated coverslips in order to capture IL-1β release from individual cells, whose viability could be determined by MitoTracker Red staining (Cullen et al., 2015). As expected, individual WT cells lost viability and released IL-1β after inflammasome activation (Figure 2D). In contrast, individual *Sarm1*$^{-/-}$ cells remained viable but still produced IL-1β after inflammasome activation (Figure 2D), demonstrating that, in the absence of SARM, IL-1 production and pyroptosis after inflammasome activation are uncoupled in individual cells. Thus, BMDMs lacking SARM behave similarly to "hyperactivated" cells that produce IL-1 but do not pyroptose after NLRP3 activation (Evavold et al., 2018; Zanoni et al., 2017).

Furthermore, cell fate after inflammasome activation could be altered by simply raising the concentration of SARM protein in cells: when WT iBMDMs were retrovirally transduced to stably express Flag-SARM (Figure 2E), NLRP3-dependent IL-1β and IL-1α release was significantly reduced (Figures 2F and 2G), whereas NLRP3-dependent LDH release was significantly increased (Figure 2H) compared to cells expressing empty vector. Hence, intracellular SARM-protein concentration affects the amount of IL-1β release and pyroptosis, and thus, SARM protein controls cell fate after NLRP3 inflammasome activation.

SARM Negatively Regulates NLRP3-Dependent Caspase-1 Activation

We next examined how SARM regulates the inflammasome to suppress IL-1 production. Absence of SARM did not inhibit the mRNA or protein expression of NLRP3 or ASC (Figures S3A–S3C). Furthermore, LPS-stimulated pro-IL-1β expression was unaltered in *Sarm1*$^{-/-}$ cells compared to WT cells (Figure 3A, third panel, compare lanes 2 and 6). In contrast, the processing of pro-IL-1β and release of mature IL-1β were increased in the absence of SARM, because, after nigericin treatment, in *Sarm1*$^{-/-}$ cells less pro-IL-1β was apparent in cell lysates (Figure 3A, third panel, compare lanes 4 and 8), while more IL-1β appeared in the supernatants (Figure 3A, top panel, compare lanes 4 and 8) compared to WT cells. Consistent with these data, *Sarm1*$^{-/-}$ cells displayed increased NLRP3-dependent caspase-1 activation compared to WT cells (Figure 3B). Thus, SARM is a negative regulator of NLRP3-activated caspase-1.

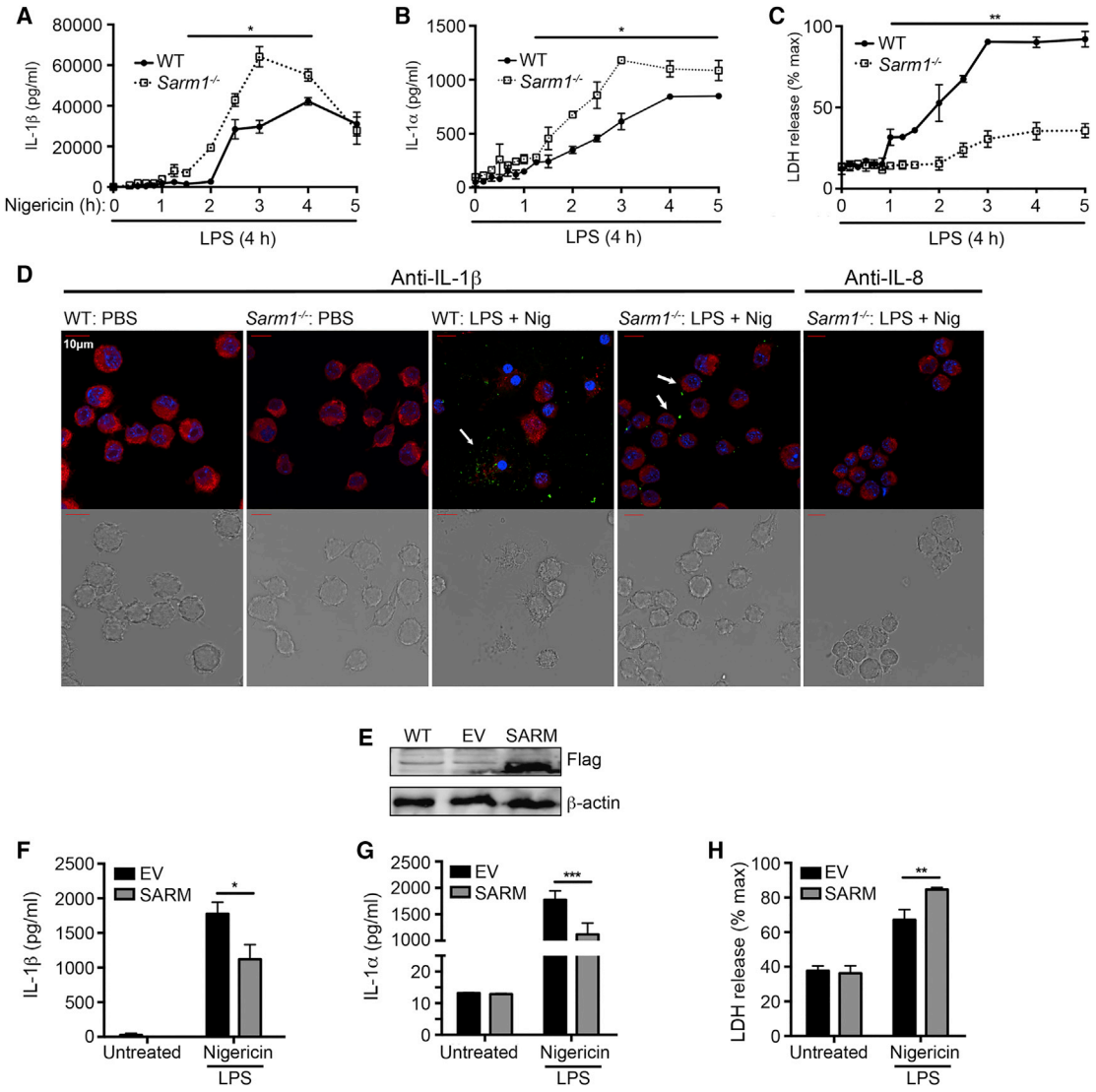

Figure 2. The Absence of SARM Uncouples Inflammasome-Dependent IL-1 Production and Pyroptosis

(A and B) ELISA of IL-1β (A) and IL-1α (B) from WT and *Sarm1*$^{-/-}$ primary BMDMs primed with LPS followed by stimulation with nigericin for the indicated times.

(C) LDH release in WT and *Sarm1*$^{-/-}$ primary BMDMs treated as described in (A).

(D) IL-1β release (green) from individual WT and *Sarm1*$^{-/-}$ iBMDM cells following NLRP3 inflammasome activation visualized using confocal microscopy. Slides were coated with anti-IL-1β detection antibody. Mitochondria are stained with MitoTracker Red and nuclei with DAPI (blue). Anti-IL-8 detection antibody was used as a negative control. Images are representative of three independent experiments. Red scale bar, 10 μm.

(E–H) WT iBMDMs were retrovirally transduced to stably express a Flag-SARM transgene. (E) Immunoblot analysis of BMDMs left untransduced (WT) or transduced with empty vector (EV) or Flag-SARM. (F and G) ELISA of IL-1β (F) and IL-1α (G) released from EV- or Flag-SARM-expressing BMDMs after activation of NLRP3. (H) LDH release assay from cells treated as in (F).

All data are mean ± SD of triplicate samples and are representative of three independent experiments. *$p < 0.05$, **$p < 0.01$, ***$p < 0.001$, ****$p < 0.0001$ (Student's t test).

SARM Interacts with NLRP3 to Inhibit ASC Oligomerization

To explore how SARM inhibits caspase-1 activation, inflammasome formation was examined. For this, inflammasome-stimulated ASC oligomerization was measured using three distinct assays and, in each case, we found that in the absence of SARM, ASC oligomerization was enhanced. Firstly, inflammasome-dependent ASC polymerization captured by protein cross-linking was markedly increased in the absence of SARM (Figure 3C). Secondly, endogenous ASC-speck formation measured by flow cytometry (Sester et al., 2015) demonstrated that a greater percentage of cells displayed detectable ASC-speck formation after nigericin treatment when SARM was deleted (Figures S4A and S4B). Finally, cells stained for endogenous ASC were observed by confocal microscopy. Here, more ASC specks were visible in the population of *Sarm1*$^{-/-}$ cells compared to

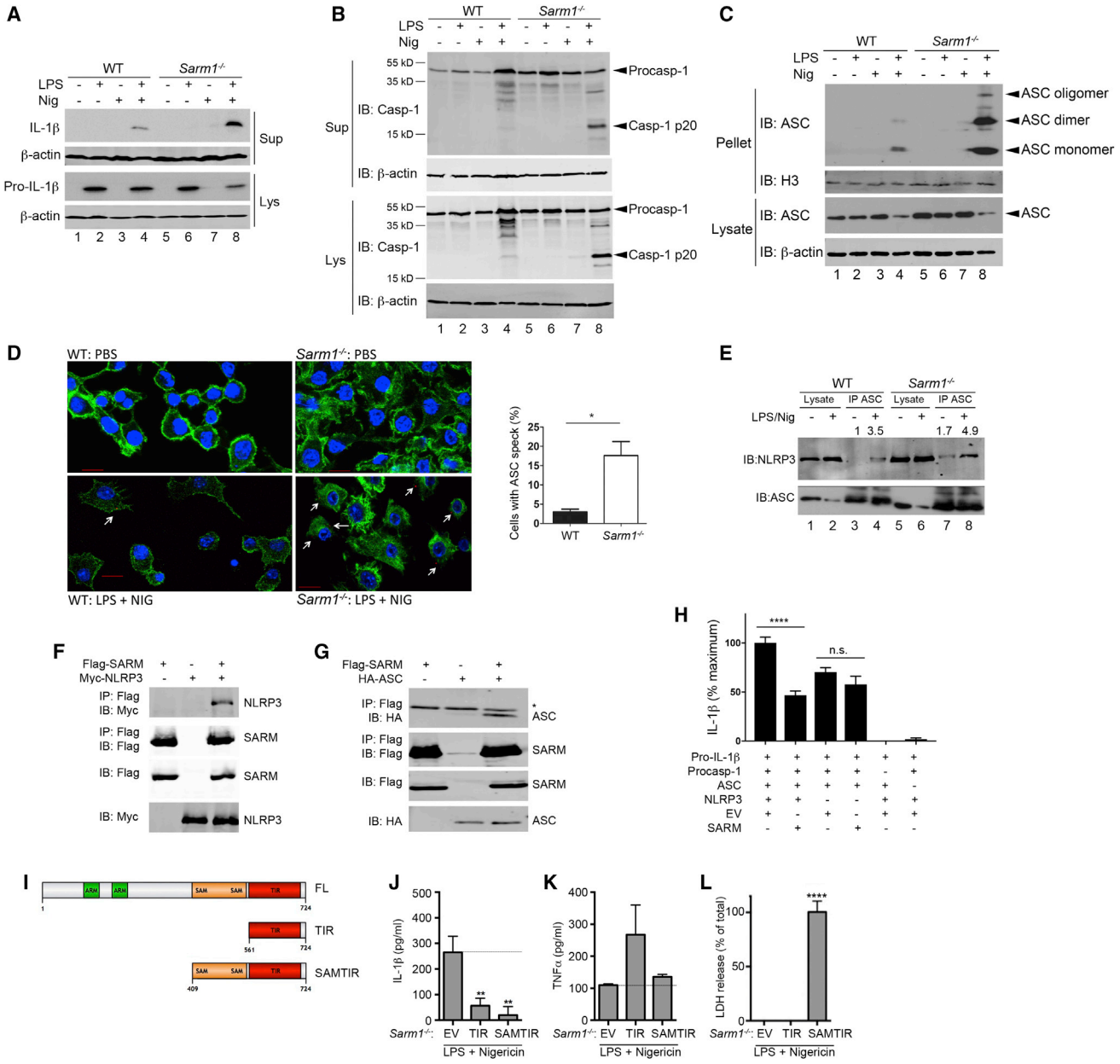

Figure 3. Negative Regulation of the NLRP3 Inflammasome by SARM via the TIR Domain

(A) SARM inhibits pro-IL-1β processing. Cell lysates and supernatants were generated from LPS-primed, nigericin-treated iBMDMs and immunoblotted for IL-1β and β-actin.

(B) SARM inhibits capsase-1 activation. Cell lysates and supernatants from cells treated as in (A) were immunoblotted for caspase-1 and β-actin.

(C) SARM inhibits ASC oligomerization. Soluble cell lysates and cross-linked cell pellets from cells treated as in (A) were immunoblotted for ASC and β-actin (loading control for cell lysates) or histone H3 (loading control for cell pellets).

(D) WT and *Sarm1*$^{-/-}$ iBMDMs seeded on coverslips were treated as in (A). Cells were fixed, permeabilized, and stained with anti-ASC antibodies to detect ASC-speck formation and visualized using confocal microscopy. Phalloidin staining of cytoskeleton (green) indicates intact *Sarm1*$^{-/-}$ cells after inflammasome activation (lower right). Images are representative of three independent experiments. Bar chart shows evaluation of the percentage of iBMDMs containing a visible ASC speck. Data are mean ± SD of three independent experiments. Red scale bar, 10 μm.

(E) Endogenous co-immunoprecipitation of ASC and NLRP3 in WT or *Sarm1*$^{-/-}$ iBMDMs following NLRP3 inflammasome activation. Numbers above lanes indicate the fold increase in NLRP3 co-immunoprecipitated (IP'd) with ASC compared to WT unstimulated cells, as assessed by densitometry (NLRP3 IP'd as a fraction of ASC IP'd).

(F and G) SARM associates with NLRP3 and ASC. Co-immunoprecipitation of Flag-SARM with Myc-NLRP3 (F) and HA-ASC (G) in HEK293T cells. * = antibody light chain.

(H) Direct inhibition by SARM of the reconstituted NLRP3 inflammasome. HEK293T cells were transfected with the indicated plasmids and IL-1β release was measured. Data are shown as a percentage of maximal IL-1β measured for fully reconstituted NLRP3 inflammasome in the absence of SARM. Data are mean ± SEM for three independent experiments, each performed in triplicate.

(legend continued on next page)

WT cells after nigericin treatment (Figure 3D). Thus, enhanced ASC oligomerization in the absence of SARM explains the heightened caspase-1 activation in *Sarm1*$^{-/-}$ cells. Further, nigericin-treated *Sarm1*$^{-/-}$ cells showed inflammasome assembly (i.e., ASC-speck formation) in intact cells (as indicated by intense phalloidin staining of the cytoskeleton [green]).

We next explored how SARM might inhibit ASC oligomerization by analyzing a number of reported cellular mechanisms associated with inflammasome regulation. Thus, we looked for reduced interferon-β (IFNβ) induction (Guarda et al., 2011), increased tubulin acetylation, or altered NLRP3 mitochondrial localization (Misawa et al., 2013) following inflammasome activation. However, no such differences were apparent in *Sarm1*$^{-/-}$ cells (Figures S3D–S3F). But when we examined the endogenous interaction between ASC and NLRP3 after inflammasome activation, we found that this was enhanced in cells lacking SARM (Figure 3E, compare lane 8 to lane 4). Furthermore, SARM could interact with both NLRP3 and ASC in human embryonic kidney (HEK) 293 cells (Figures 3F and 3G). Therefore, SARM normally suppresses the association between ASC and NLRP3, likely through direct interactions with one or both proteins.

To examine the direct effect of SARM on NLRP3, the inflammasome was reconstituted in HEK293 cells by transfection of cells with pro-IL-1β, pro-caspase-1, ASC, and NLRP3 (Figure S5). Under these conditions, the inflammasome is active to cause IL-1β secretion without external stimulus (Shi et al., 2016). Expression of ASC led to pro-caspase-1-dependent secretion of IL-1β (Figure 3H), presumably due to self-association leading to capsase-1 activation. IL-1β secretion was further enhanced by addition of NLRP3 (Figure 3H). Expression of SARM inhibited NLRP3-dependent, but not NLRP3-independent (triggered by ASC in the absence of NLRP3), IL-1β release (Figure 3H). Of note, in this inflammasome reconstitution assay, IL-1β release is independent of cell lysis (Figure S5). Together, these data show that SARM interacts with NLRP3 to suppress ASC-speck formation and caspase-1 activation.

We next determined which domains of SARM were required for inflammasome inhibition by retroviral expression of different SARM truncations in *Sarm1*$^{-/-}$ iBMDMs (Figure 3I). This showed that the TIR domain alone was sufficient to significantly inhibit IL-1β (Figure 3J), while TNF release was not suppressed (Figure 3K). In contrast, both the sterile alpha motif (SAM) domain, required for SARMs ability to multimerize (Gerdts et al., 2013), and the TIR domain were required for SARM to stimulate pyroptosis in *Sarm1*$^{-/-}$ iBMDMs (Figure 3L), suggesting that the mechanism whereby SARM negatively regulates NLRP3-mediated caspase-1 activation and pyroptosis are distinct (see below).

SARM Regulates the Non-canonical Inflammasome and Contributes to LPS-Induced Sepsis

Intracellular LPS activates a caspase-11-dependent non-canonical inflammasome implicated in sepsis, leading to both IL-1 production and pyroptosis (Kayagaki et al., 2011). Because caspase-11-dependent IL-1β release is also NLRP3 dependent (Kayagaki et al., 2011), we assessed whether SARM would also affect the non-canonical inflammasome. LPS-primed WT and *Sarm1*$^{-/-}$ iBMDMs were transfected with LPS, showing that, in *Sarm1*$^{-/-}$ iBMDMs, IL-1β secretion markedly increased compared to WT cells, whereas TNF did not and was, in fact, partially suppressed (Figures 4A and 4B). Similar to caspase-1-dependent cell death (Figure 1), in response to transfected LPS, pyroptosis was significantly reduced in cells lacking SARM compared to WT cells (Figure 4C), whereas absence of SARM did not affect caspase-11 protein expression (Figure S3G).

Because pyroptosis triggered by caspase-11 activation by intracellular LPS mediates LPS-induced sepsis *in vivo* (Deng et al., 2018; Yang et al., 2015), we tested whether absence of SARM affected this response. Following intraperitoneal injection of LPS, *Sarm1*$^{-/-}$ mice displayed significantly improved temperature change (Figure 4D), clinical score (Figure 4E), and survival (Figure 4F) compared to WT animals. Protection in *Sarm1*$^{-/-}$ mice is consistent with the notion that LPS-mediated sepsis is driven by pyroptosis rather than by IL-1β release (Yang et al., 2015), and indeed, the amounts of systemic pro-inflammatory cytokines detected were similar in WT and *Sarm1*$^{-/-}$ mice (Figure 4G).

SARM Is Required for Inflammasome-Stimulated Mitochondrial Depolarization

The data so far showed that SARM suppresses NLRP3-dependent IL-1β release by directly targeting NLRP3 via the TIR domain, yet how SARM contributes to both caspase-1- and caspase-11-mediated pyroptosis remained to be established. To address this, we first examined GSDMD cleavage, which, in both cases, is necessary for pyroptosis (He et al., 2015; Kayagaki et al., 2015; Shi et al., 2015). Although caspase-dependent GSDMD cleavage was originally thought to be sufficient for pyroptosis, recent work shows that this is not the case, because in some cases, after inflammasome activation, cells can release IL-1β through GSDMD pores without pyroptosing (Evavold et al., 2018; Heilig et al., 2018; Monteleone et al., 2018). Here, GSDMD cleavage was not compromised in nigericin-stimulated *Sarm1*$^{-/-}$ BMDMs but was in fact increased (Figure 5A), consistent with the more activate caspase-1 observed in *Sarm1*$^{-/-}$ BMDMs (Figure 3B). Thus, reduced pyroptosis in *Sarm1*$^{-/-}$ cells was not due to impaired GSDMD cleavage.

We wondered what other cellular process that would be lacking in *Sarm1*$^{-/-}$ cells was required for NLRP3-dependent pyroptosis apart from GSDMD cleavage. To begin to gain insight into this, we next determined where in BMDMs SARM was located. We found that SARM was located specifically at the mitochondria (Figure 5B), and neither LPS priming nor inflammasome activation by nigericin treatment affected this localization. However, treatment of LPS-primed cells with

(I–L) The SARM TIR domain is required for inhibition of IL-1 production. Schematic of SARM truncations (I) retrovirally expressed in *Sarm1*$^{-/-}$ iBMDMs prior to NLRP3 inflammasome activation and measurement of IL-1β (J), TNFα (K), and pyroptosis (L). Data are mean ± SD of triplicate samples and are representative of two independent experiments.

In (A) to (C) and (E) to (G), immunoblots are representative of three independent experiments. *$p < 0.05$, **$p < 0.01$, ***$p < 0.001$, ****$p < 0.0001$, n.s. not significant (Student's t test). See also Figures S3, S4, and S5.

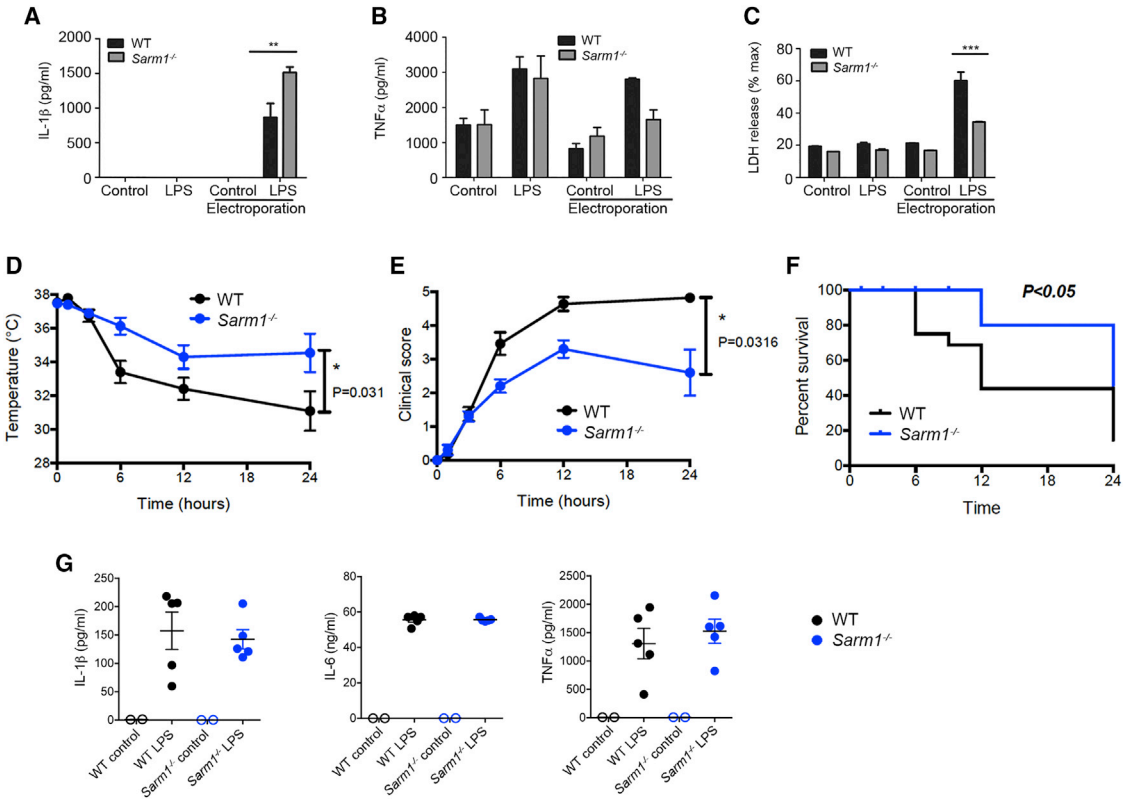

Figure 4. SARM Regulates Cell Fate after Non-canonical Inflammasome Activation and *Sarm1*$^{-/-}$ Mice Show Decreased Mortality in a Model of LPS-Induced Endotoxic Shock

(A–C) WT or *Sarm1*$^{-/-}$ iBMDMs were all primed with LPS and then stimulated with LPS, electroporated with LPS, or left untreated (Control) as indicated for 16 h before IL-1β (A) and TNFα (B) were measured by ELISA or cell death was measured by LDH release (C). Data are mean ± SD of triplicate samples and are representative of 3 independent experiments. **$p < 0.01$, ***$p < 0.001$ (Student's t test).

(D–F) Endotoxic shock was induced in groups of male WT C57 and age-matched *Sarm1*$^{-/-}$ C57 mice by i.p. injection of 10 mg/kg ultra-pure (UP) LPS. Body temperature (D), clinical signs of shock (E), and mortality (F) were monitored for 24 h after LPS injection. Data are representative of two independent experiments of 5 to 6 mice per group (mean ± SEM, *$p < 0.05$). p value for survival curve, 0.0308. Statistical analysis compared area-under-curve (D and E) difference by Student's t test (D and E) or statistical analysis of the survival curve (F) by a Kaplan-Meier test.

(G) Serum cytokines were analyzed in mice 3 h after injection of 10 mg/kg UP-LPS. Data are representative of two independent experiments of 2 to 5 mice per group (mean ± SEM).

See also Figure S3.

nigericin did cause an altered pattern of staining of SARM whereby SARM staining at the mitochondria appeared more intense and punctate, leading to strong overlap with Mito-Tracker Red (Figure 5C). This suggested SARM clustering at the mitochondria after inflammasome activation by nigericin, since cells stimulated with LPS alone or nigericin alone appeared similar to control cells (Figure 5C). In T cells, SARM triggers apoptotic cell death by activating MDP (Panneerselvam et al., 2013). Because MDP has also been proposed to contribute to NLRP3-dependent pyroptosis (Yu et al., 2014) and is observed after caspase-11 activation prior to pyroptosis (de Vasconcelos et al., 2019), we examined whether there was a role for SARM in mediating MDP after inflammasome activation. Nigericin treatment of cells after LPS priming did indeed lead to MDP in WT iBMDMs, and compellingly, this was significantly reduced in cells lacking SARM (Figures 5D and 5E). Thus, we propose that, upon inflammasome activation, SARM clusters at the mitochondria and triggers MDP, which contributes to pyroptosis.

Hyperactivating NLRP3 Stimulants Do Not Cause Mitochondrial SARM Clustering or MDP

Viable *Sarm1*$^{-/-}$ BMDMs post nigericin stimulation resembled macrophages stimulated with hyperactivating NLRP3 stimulants (Evavold et al., 2018) in that inflammasome speck formation occurred (Figure 3D), GSDMD cleavage proceeded (Figure 5A), and IL-1β release occurred (Figure 2D). Such NLRP3 stimulants, like peptidoglycan (PGN), cause IL-1β secretion from living cells after inflammasome activation (Evavold et al., 2018). However, to date, cell-intrinsic mechanisms that explain why some NLRP3 activators (e.g., nigericin) cause both cell death and cytokine release, while others (e.g., PGN) only cause cytokine release, have not been uncovered. Therefore, we tested the hypothesis that inflammasome-stimulated SARM clustering at the mitochondria and SARM-dependent MDP would be distinguishing features of activators that cause cell lysis compared to those that don't.

To test this, we first confirmed that nigericin and PGN treatment of BMDMs led to different cell-fate outcomes. LPS-primed BMDMs treated with nigericin displayed robust LDH release and

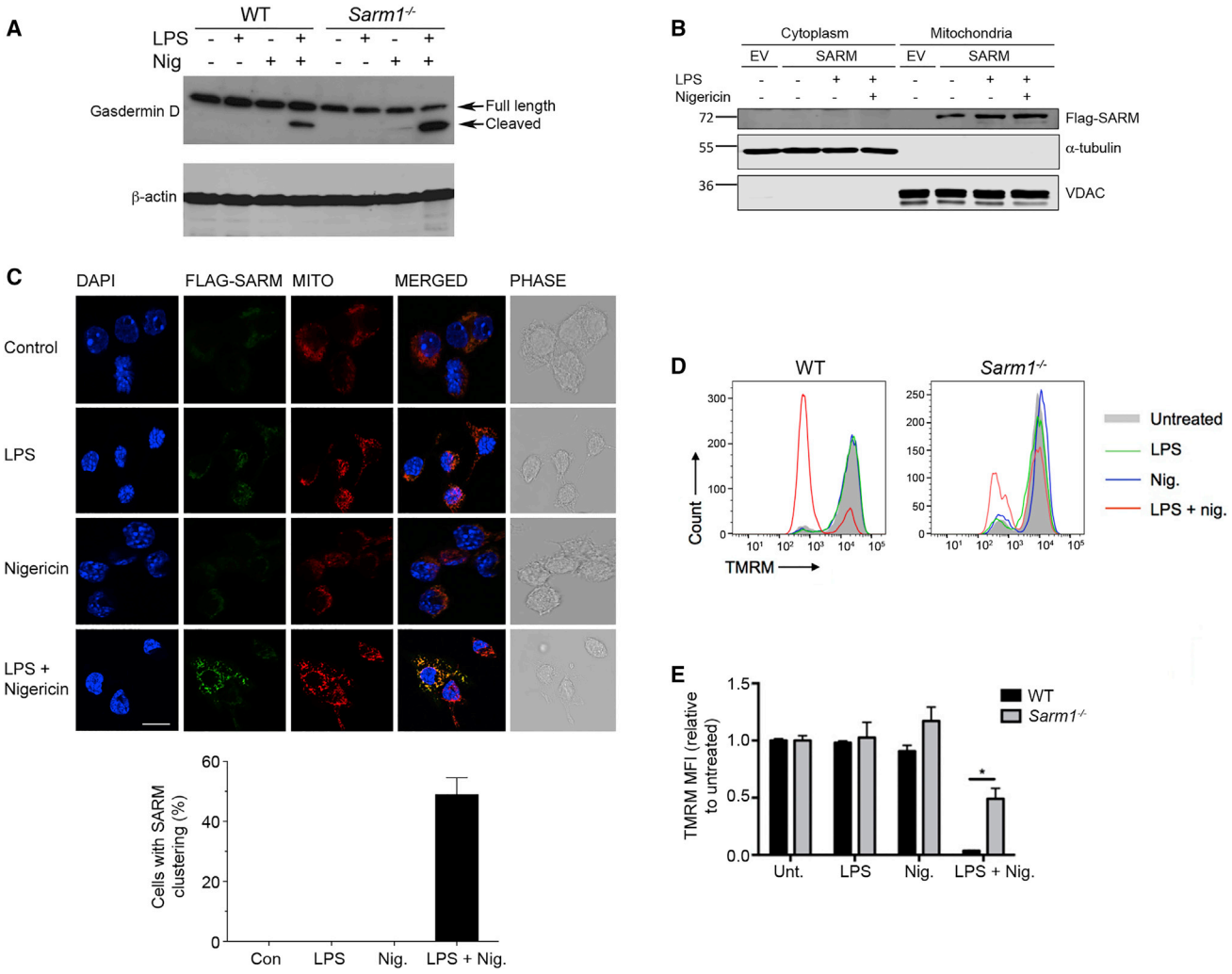

Figure 5. SARM Is Required for Inflammasome-Dependent Mitochondrial Depolarization

(A) Gasdermin D cleavage is not prevented in the absence of SARM. Gasdermin D cleavage was assessed by immunoblot in WT and *Sarm1*$^{-/-}$ primary BMDMs treated as indicated. Immunoblots are representative of three independent experiments.

(B) SARM resides at the mitochondria before and after stimulation. Mitochondrial and cytosolic fractions were generated from *Sarm1*$^{-/-}$ iBMDMs stably expressing Flag-SARM or empty vector (EV) that had been treated with LPS and nigericin as indicated. Samples were immunoblotted for Flag-SARM, voltage-dependent anion channel (VDAC), and α-tubulin. Blot is representative of four independent experiments.

(C) SARM clusters at the mitochondria after inflammasome activation. Flag-SARM-expressing iBMDMs were untreated as indicated, and SARM localization was visualized using confocal microscopy. Flag-SARM is stained green, mitochondria are stained using MitoTracker Red, and nuclei are stained using DAPI (blue). Images are representative of three independent experiments. Bar chart shows evaluation of the percentage of SARM-positive cells that show SARM clustering at the mitochondria. Data are mean ± SD of three independent experiments. White scale bar, 10 μm.

(D and E) Mitochondrial depolarization was measured in WT and *Sarm1*$^{-/-}$ iBMDMs treated as indicated. Data are mean ± SD of triplicate samples and are representative of three independent experiments. *$p < 0.05$ (Student's t test).

IL-1β secretion, whereas the same BMDMs treated with PGN showed no LDH release above unstimulated cells, even after prolonged exposure, yet did secrete significant amounts of IL-1β (Figures 6A and 6B). Compared to nigericin, PGN caused no clustering of SARM at the mitochondria (Figure 6C). To accurately compare MDP in nigericin- and PGN-treated cells, we gated for MitoTracker-Green-positive cells in order to examine tetramethylrhodamine, methyl ester (TMRM) loss in mitochondria that are intact. This showed that LPS-primed cells treated with nigericin showed increased MDP compared to untreated cells, whereas primed cells treated with PGN did not (Figures 6D and 6E).

Therefore, mitochondrial SARM clustering and SARM-dependent MDP distinguish NLRP3 activators that cause pyroptosis and those that do not, and as such, SARM modulation represents a cell-intrinsic mechanism to regulate different cell-fate outcomes after inflammasome activation (Figure S6).

DISCUSSION

The data presented here indicate that SARM has a role in regulating cell fate after activation of the NLRP3 inflammasome. Specifically, we have shown that: (1) SARM, a mammalian

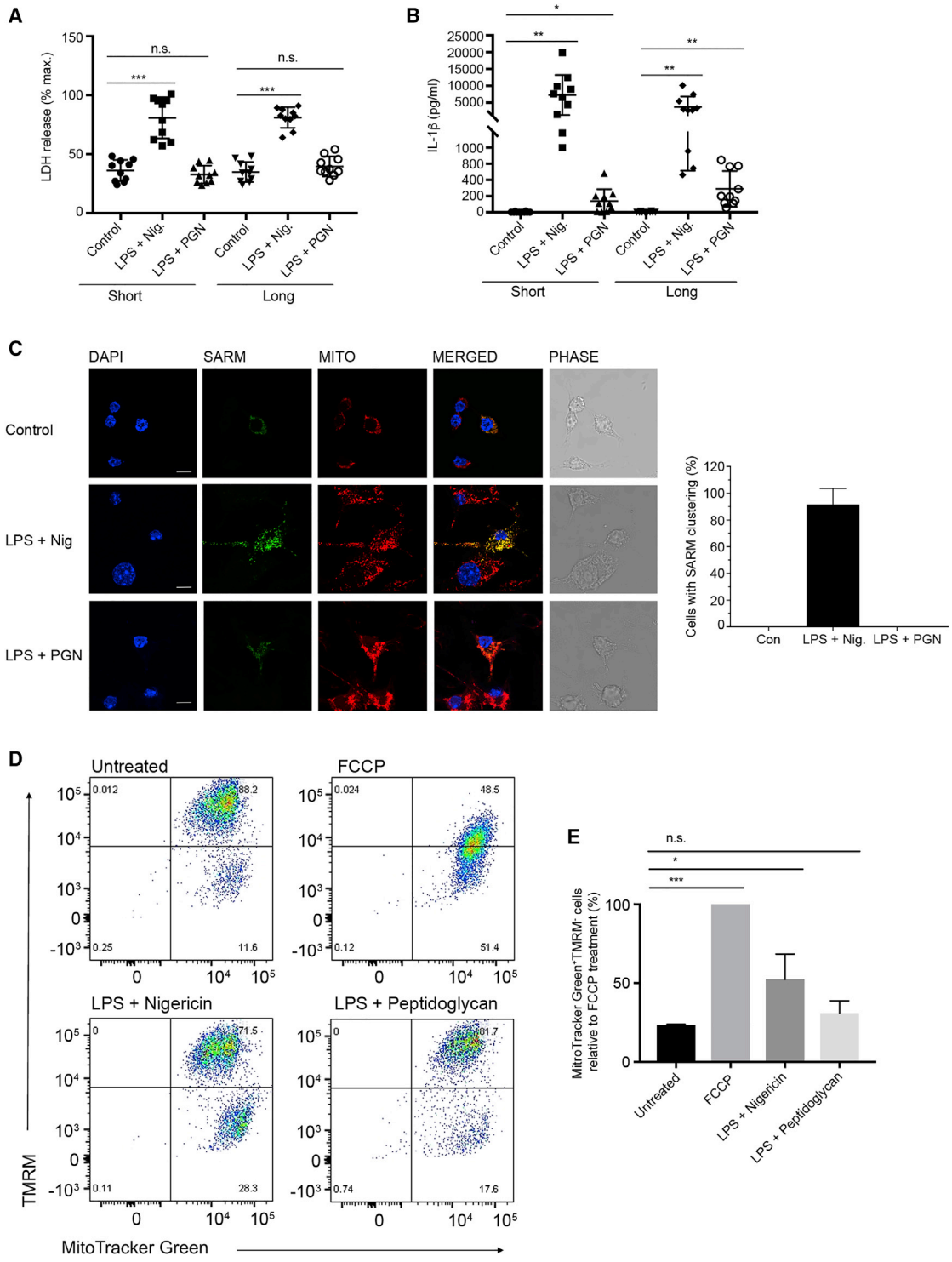

Figure 6. An NLRP3 Hyperactivating Stimulant Does Not Cause SARM Clustering or Mitochondrial Depolarization

(A and B) Primary BMDMs were seeded at 5 × 10^5 cells/mL and left overnight to adhere. Cells were primed with 200 ng/mL of LPS for 4 h and either treated with 10 μM nigericin for 3 h (short) or 20 h (long) or with 50 μg/mL peptidoglycan for 6 h (short) or 20 h (long). Pyroptosis was assessed by LDH release (A) and IL-1β (B) was measured. All data are mean ± SEM of ten independent experiments performed in technical triplicates.

(C) *Sarm1*$^{-/-}$ iBMDMs stably expressing Flag-SARM were grown on coverslips, primed with 200 ng/mL of LPS for 4 h, and either treated with 10μM nigericin for 1 h or 50 μg/mL peptidoglycan for 6 h. Flag-SARM was detected by Alexafluor 488, and mitochondria were stained using MitoTracker Red and nuclei stained using DAPI. The cells were examined using confocal microscopy. Images are representative of three independent experiments. Bar chart shows evaluation of the percentage of SARM-positive cells that show SARM clustering at the mitochondria. Data are mean ± SD of two independent experiments. White scale bar, 8 μm.

(legend continued on next page)

TIR-domain-containing protein, negatively regulates the NLRP3 inflammasome via its TIR domain to suppress capsase-1 activation and IL-1β release. (2) In response to NLRP3 activation, cells can be rendered hyperactivated rather than pyroptotic by removal of SARM. This was observed at the single-cell level, where cells lacking SARM remained intact and viable yet produced IL-1β. Nigericin-treated *Sarm1*$^{-/-}$ cells showed inflammasome assembly (i.e., ASC-speck formation) in intact cells, reminiscent of what has been seen after treating cells with NLRP3 hyperactivating ligands (Evavold et al., 2018). (3) Simply increasing SARM protein expression by retroviral transduction of macrophages uncoupled cytokine release and cell death, leading to reduced IL-1 release and increased pyroptosis. (4) SARM mediates inflammasome-dependent MDP. (5) An NLRP3 activator that causes cell hyperactivation does not cause mitochondrial SARM clustering or MDP. (6) SARM contributes to LPS-induced sepsis *in vivo*. The fact that *Sarm1*$^{-/-}$ mice were protected in an LPS model of sepsis suggests that pyroptotic cell death contributes more to LPS lethality than IL-1 release does. Consistent with that, other investigators showed that LPS-induced lethality is mediated by caspase-11-dependent pyroptosis and not caspase-1-dependent IL-1β release (Kayagaki et al., 2011; Yang et al., 2015).

Similar to IL-1β, we showed that, in macrophages lacking SARM, IL-1α release is also increased. Although IL-1α is processed from its pro form to an active form in a caspase-1-independent manner by the calpains, reports suggest that caspase-1 does have a role in IL-1α secretion (Zheng et al., 2013). This is consistent with our observation of enhanced IL-1α production in macrophages lacking SARM that display increased caspase-1 activity. Thus, similar to IL-1β, release of IL-1α from BMDMs is not completely dependent on cell lysis because increased release of IL-1α occurs in the background of reduced cell death in macrophages lacking SARM.

The notion that release of IL-1 is intrinsically dependent on cell death has been debated in recent years, but this idea gained weight again with the discovery that cleavage of GSDMD by caspase-1 led to the formation of plasma-membrane pores comprising the cleaved N-terminal domain of GSDMD and that GSDMD was required for pyroptosis. Another line of evidence for this is based on the tight temporal coupling of IL-1β release to the loss of plasma-membrane integrity and the fact that cell lysis is often the ultimate fate of IL-1β-producing macrophages. Although in some cell types, such as human THP-1 monocytes (Cullen et al., 2015), IL-1β release is coupled to cell death, our work here adds to the growing body of literature showing that IL-1β production is not intrinsically dependent on pyroptosis (Chen et al., 2014; Conos et al., 2016; Gaidt et al., 2016; Zanoni et al., 2016). Furthermore, it is now accepted that GSDMD pores are necessary, but not sufficient, for the osmotic collapse of cells that leads to pyroptosis, and the pores themselves can be regulated by membrane-repair mechanisms after caspase-1 activation (Rühl et al., 2018). Coupled to this, GSDMD pores can facilitate IL-1β release from living cells treated with NLRP3 hyperactivating stimulants such as PGN (Evavold et al., 2018; Heilig et al., 2018), and GSDMD-independent mechanisms of IL-1β release also exist (Monteleone et al., 2018). Thus, cell-intrinsic mechanisms to regulate cell fate after inflammasome activation, independent of GSDMD pore formation—which would define, for example, why hyperactivating ligands cause NLRP3-dependent IL-1β release without pyroptosis—remain to be defined. SARM represents one such mechanism, being a key regulator of inflammasome activation in macrophages by acting as a gatekeeper controlling the balance between IL-1 production and pyroptosis.

As regards how SARM restrains caspase-1 activation to suppress IL-1β, SARM directly targeted NLRP3 activation to suppress recruitment of ASC and, hence, ASC-speck formation. Many studies have proposed specific mechanisms whereby NLRP3 is activated by diverse stimulants to oligomerize and cluster with ASC. Recently, oxidized mtDNA has been implicated as a direct ligand for NLRP3 that would be formed in response to diverse activators and would promote NLRP3 inflammasome assembly upon binding (Zhong et al., 2018). In contrast, another very recent study showed that multiple activators of NLRP3 lead to disassembly of the *trans*-Golgi network which facilitated NLRP3 aggregation and subsequent oligomerization of ASC (Chen and Chen, 2018). Although it is currently difficult to reconcile these studies and integrate them into previous proposed mechanisms for NLRP3 activation, what is clear is that NLRP3 activation leads to association with ASC to facilitate ASC-speck formation, and this step was clearly targeted by SARM. Where exactly SARM engages with NLRP3 within cells to restrain ASC-speck formation remains to be determined, and this is a challenging issue to resolve, given the inability to detect endogenous SARM by immunodetection. In the light of recent developments that show active NLRP3 co-migrating with the *trans*-Golgi network, future work will determine whether a small fraction of SARM distinct from the mitochondrial fraction is contained within the *trans*-Golgi network fraction or whether SARM restraining of NLRP3 occurs from the mitochondrial fraction. Reconstitution of the NLRP3 inflammasome in HEK293T cells showed that SARM directly targeted NLRP3 to suppress IL-1β release. Further, we showed that relief of inhibition of pro-IL-1β processing by removal of SARM led to increased IL-1β release. This is entirely consistent with the recent demonstration by Schroder and colleagues that the key control point for IL-1β release is pro-IL-1β cleavage, since IL-1β cleavage by caspase-1 was both necessary and sufficient for both GSDMD-dependent and -independent IL-1β secretion (Monteleone et al., 2018).

Thus, in macrophages, SARM acts as a brake to control and restrain the formation of the multi-protein NLRP3 inflammasome complex. The three defined protein domains of SARM, namely the ARM repeats, the two SAM domains, and the TIR domain, are all motifs capable of facilitating interactions with other proteins (Carty and Bowie, 2019). We found that expression of the TIR domain of SARM was sufficient to inhibit IL-1β production. The TIR domain of SARM is distinct from TIR domains in other

(D and E) WT iBMDMs were primed with 200 ng/mL of LPS for 4 h and either treated with 10 μM nigericin for 1 h or 50 μg/mL peptidoglycan for 6 h. Cells were stained with TMRM and MitoTracker Green (MTG) and analyzed using LSRFortessa. Flow cytometry plots are representative of three independent experiments (D). Bar chart is mean ± S.D. (n = 3) showing percentage of cells relative to FCCP treatment that are MTG positive and TMRM negative (E).
*p < 0.05, **p < 0.01, ***p < 0.001, n.s., no significant difference (Student's *t* test). See also Figure S6.

mammalian proteins and is more closely related to bacterial TIR proteins such as *E. coli* TcpC (Zhang et al., 2011). Of note, TcpC, like SARM, was shown to inhibit NLRP3 inflammasome activation via its TIR domain binding to NLRP3 (Waldhuber et al., 2016), providing evidence that a subset of TIR domains have NLRP3-targeting ability.

In contrast to NLRP3 inhibition, our data show that, to drive pyroptosis, both the SAM and TIR domains of SARM are required. After nigericin-mediated activation of the NLRP3 inflammasome, SARM clustered at the mitochondria. Because the SAM motifs of SARM are known to be required for its oligomerization (Gerdts et al., 2013) and here shown to be required for pyroptosis, SARM may oligomerize at the mitochondria after NLRP3 activation to facilitate MDP. How exactly SARM clustering facilitates MDP and how MDP contributes to NLRP3-dependent pyroptosis remains to be determined, but it is likely that SARM-dependent MDP is a cellular insult that is required to progress GSDMD pore-expressing macrophages to full pyroptosis. One possibility is that MDP leads to energy collapse in cells, which would restrain membrane repair and allow pyroptosis to proceed. Thus, *Sarm1*$^{-/-}$ cells may display enhanced membrane repair. However, membrane repair after NLRP3 activation has been shown to inhibit both pyroptosis and IL-1β release (Rühl et al., 2018), so this would not account for the increased IL-1β release in the absence of SARM. Other groups have also shown that MDP occurs after NLRP3 activation (Yu et al., 2014; Zhong et al., 2018) and that pyroptosis triggered by intracellular LPS via capsase-11 is characterized by MDP prior to the loss of plasma-membrane integrity (de Vasconcelos et al., 2019). Further, SARM-dependent MDP may be of relevance to other forms of macrophage cell death, since we found induction of necroptosis and of apoptosis by some stimulants was suppressed in *Sarm1*$^{-/-}$ cells (data not shown).

The fact that NLRP3 activation led to MDP and that this depolarization was SARM-dependent suggests a model whereby inflammasome activation causes SARM oligomerization at the mitochondria to cause MDP, which facilitates pyroptosis. As articulated by Próchnicki and Latz (2017), not all stimuli that cause inflammasome assembly and caspase-1 activation also elicit pyroptosis, but the underlying mechanisms of this "protection" from pyroptosis is unknown. Here, we found that PGN, a hyperactivating NLRP3 agonist that causes IL-1 release without cell death, failed to cause SARM clustering or MDP. This absence of SARM-dependent MDP represents a cell-intrinsic mechanism to protect cells from pyroptosis after NLRP3 activation. Why nigericin but not PGN causes SARM clustering and SARM-dependent MDP is still unclear, and whether this is a qualitative or quantitative difference in signal remains to be fully determined.

More broadly, because the absolute amount of SARM protein in BMDMs defined the exact cell-fate outcome (IL-1 release versus pyroptosis), it is conceivable that the concentration of intracellular SARM could fine-tune inflammasome outcomes in multiple cell types. The fact that inflammasome activation in some contexts leads to cytokine production without pyroptosis (Chen et al., 2014; Conos et al., 2016; Gaidt et al., 2016; Zanoni et al., 2016) might be accounted for by low or absent expression of SARM or signal-induced SARM down-regulation, but this remains to be investigated. Overall, we propose that SARM modulation of IL-1β and pyroptosis represents the first cell-intrinsic mechanism to regulate cell fate outcomes after NLRP3 inflammasome activation.

STAR★METHODS

Detailed methods are provided in the online version of this paper and include the following:

- KEY RESOURCES TABLE
- CONTACT FOR REAGENT AND RESOURCE SHARING
- EXPERIMENTAL MODEL AND SUBJECT DETAILS
  - Mice
  - Cell culture
  - Retroviral transduction of iBMDM
  - Generation of *Sarm1*$^{-/-}$ iBMDMs stably expressing SARM
  - Induction of LPS-induced sepsis
- METHOD DETAILS
  - Inflammasome activation and analysis
  - Immunoblotting
  - RNA analysis by quantitative RT-PCR
  - Enzyme-linked immunosorbent assay
  - ASC oligomerization assay
  - Visualization of ASC speck formation using confocal microscopy
  - Analysis of ASC speck formation by flow cytometry
  - Visualization of SARM localization after inflammasome activation
  - Analysis of SARM clustering by confocal microscopy
  - Isolation of mitochondria
  - Visualization of IL-1β secretion from single cells
  - Co-immunoprecipitation of proteins
  - Reconstitution of NLRP3 inflammasome in HEK293T cells
  - Analysis of mitochondrial depolarization
- QUANTIFICATION AND STATISTICAL ANALYSIS

SUPPLEMENTAL INFORMATION

Supplemental Information can be found online at https://doi.org/10.1016/j.immuni.2019.04.005.

ACKNOWLEDGMENTS

We thank Sarah Cannon for her assistance with genotyping of the *Sarm1*$^{-/-}$ mice. This work was supported by Science Foundation Ireland (11/PI/1056 and 16/IA/4376 to A.G.B.; 10/IN.1/B3004 to P.G.F.) and by a Biotechnology and Biological Sciences Research Council-Science Foundation Ireland joint award (BBSRC-SFI, BB/P020194/1 to A.G.B.).

AUTHOR CONTRIBUTIONS

Conceptualization, A.G.B. and M.C.; Investigation, M.C., J.K., K.A.S., E.H., D.C., R.S., C.G.D., C.G.; Resources, N.M.-W., K.A.F. and E.C.L.; Writing – Original Draft, A.G.B. and M.C.; Writing – Review and Editing, A.G.B., M.C., R.S., K.A.S. and C.G.D.; Supervision, A.G.B., E.C.L., P.G.F.; Funding Acquisition, A.G.B.

DECLARATION OF INTERESTS

The authors declare no competing interests.

Received: December 21, 2018
Revised: March 12, 2019
Accepted: April 9, 2019
Published: May 7, 2019

REFERENCES

Aglietti, R.A., Estevez, A., Gupta, A., Ramirez, M.G., Liu, P.S., Kayagaki, N., Ciferri, C., Dixit, V.M., and Dueber, E.C. (2016). GsdmD p30 elicited by caspase-11 during pyroptosis forms pores in membranes. Proc. Natl. Acad. Sci. USA *113*, 7858–7863.

Broz, P., and Dixit, V.M. (2016). Inflammasomes: mechanism of assembly, regulation and signalling. Nat. Rev. Immunol. *16*, 407–420.

Carty, M., and Bowie, A.G. (2019). SARM: From immune regulator to cell executioner. Biochem. Pharmacol. *161*, 52–62.

Carty, M., Goodbody, R., Schröder, M., Stack, J., Moynagh, P.N., and Bowie, A.G. (2006). The human adaptor SARM negatively regulates adaptor protein TRIF-dependent Toll-like receptor signaling. Nat. Immunol. *7*, 1074–1081.

Chen, J., and Chen, Z.J. (2018). PtdIns4P on dispersed trans-Golgi network mediates NLRP3 inflammasome activation. Nature *564*, 71–76.

Chen, K.W., Groß, C.J., Sotomayor, F.V., Stacey, K.J., Tschopp, J., Sweet, M.J., and Schroder, K. (2014). The neutrophil NLRC4 inflammasome selectively promotes IL-1β maturation without pyroptosis during acute Salmonella challenge. Cell Rep. *8*, 570–582.

Chinnakannan, S.K., Nanda, S.K., and Baron, M.D. (2013). Morbillivirus v proteins exhibit multiple mechanisms to block type 1 and type 2 interferon signalling pathways. PLoS ONE *8*, e57063.

Coll, R.C., Robertson, A.A., Chae, J.J., Higgins, S.C., Muñoz-Planillo, R., Inserra, M.C., Vetter, I., Dungan, L.S., Monks, B.G., Stutz, A., et al. (2015). A small-molecule inhibitor of the NLRP3 inflammasome for the treatment of inflammatory diseases. Nat. Med. *21*, 248–255.

Conos, S.A., Lawlor, K.E., Vaux, D.L., Vince, J.E., and Lindqvist, L.M. (2016). Cell death is not essential for caspase-1-mediated interleukin-1β activation and secretion. Cell Death Differ. *23*, 1827–1838.

Cullen, S.P., Kearney, C.J., Clancy, D.M., and Martin, S.J. (2015). Diverse Activators of the NLRP3 Inflammasome Promote IL-1β Secretion by Triggering Necrosis. Cell Rep. *11*, 1535–1548.

de Vasconcelos, N.M., Van Opdenbosch, N., Van Gorp, H., Parthoens, E., and Lamkanfi, M. (2019). Single-cell analysis of pyroptosis dynamics reveals conserved GSDMD-mediated subcellular events that precede plasma membrane rupture. Cell Death Differ. *26*, 146–161.

Deng, M., Tang, Y., Li, W., Wang, X., Zhang, R., Zhang, X., Zhao, X., Liu, J., Tang, C., Liu, Z., et al. (2018). The Endotoxin Delivery Protein HMGB1 Mediates Caspase-11-Dependent Lethality in Sepsis. Immunity *49*, 740–753.e7.

Ding, J., Wang, K., Liu, W., She, Y., Sun, Q., Shi, J., Sun, H., Wang, D.C., and Shao, F. (2016). Pore-forming activity and structural autoinhibition of the gasdermin family. Nature *535*, 111–116.

Evavold, C.L., Ruan, J., Tan, Y., Xia, S., Wu, H., and Kagan, J.C. (2018). The Pore-Forming Protein Gasdermin D Regulates Interleukin-1 Secretion from Living Macrophages. Immunity *48*, 35–44.e6.

Gaidt, M.M., Ebert, T.S., Chauhan, D., Schmidt, T., Schmid-Burgk, J.L., Rapino, F., Robertson, A.A., Cooper, M.A., Graf, T., and Hornung, V. (2016). Human Monocytes Engage an Alternative Inflammasome Pathway. Immunity *44*, 833–846.

Gerdts, J., Summers, D.W., Sasaki, Y., DiAntonio, A., and Milbrandt, J. (2013). Sarm1-mediated axon degeneration requires both SAM and TIR interactions. J. Neurosci. *33*, 13569–13580.

Gross, O., Yazdi, A.S., Thomas, C.J., Masin, M., Heinz, L.X., Guarda, G., Quadroni, M., Drexler, S.K., and Tschopp, J. (2012). Inflammasome activators induce interleukin-1α secretion via distinct pathways with differential requirement for the protease function of caspase-1. Immunity *36*, 388–400.

Guarda, G., Braun, M., Staehli, F., Tardivel, A., Mattmann, C., Förster, I., Farlik, M., Decker, T., Du Pasquier, R.A., Romero, P., and Tschopp, J. (2011). Type I interferon inhibits interleukin-1 production and inflammasome activation. Immunity *34*, 213–223.

Guo, H., Callaway, J.B., and Ting, J.P. (2015). Inflammasomes: mechanism of action, role in disease, and therapeutics. Nat. Med. *21*, 677–687.

Gürtler, C., Carty, M., Kearney, J., Schattgen, S.A., Ding, A., Fitzgerald, K.A., and Bowie, A.G. (2014). SARM regulates CCL5 production in macrophages by promoting the recruitment of transcription factors and RNA polymerase II to the Ccl5 promoter. J. Immunol. *192*, 4821–4832.

Hams, E., Saunders, S.P., Cummins, E.P., O'Connor, A., Tambuwala, M.T., Gallagher, W.M., Byrne, A., Campos-Torres, A., Moynagh, P.M., Jobin, C., et al. (2011). The hydroxylase inhibitor dimethyloxallyl glycine attenuates endotoxic shock via alternative activation of macrophages and IL-10 production by B1 cells. Shock *36*, 295–302.

He, W.T., Wan, H., Hu, L., Chen, P., Wang, X., Huang, Z., Yang, Z.H., Zhong, C.Q., and Han, J. (2015). Gasdermin D is an executor of pyroptosis and required for interleukin-1β secretion. Cell Res. *25*, 1285–1298.

Heilig, R., Dick, M.S., Sborgi, L., Meunier, E., Hiller, S., and Broz, P. (2018). The Gasdermin-D pore acts as a conduit for IL-1β secretion in mice. Eur. J. Immunol. *48*, 584–592.

Hou, Y.J., Banerjee, R., Thomas, B., Nathan, C., García-Sastre, A., Ding, A., and Uccellini, M.B. (2013). SARM is required for neuronal injury and cytokine production in response to central nervous system viral infection. J. Immunol. *191*, 875–883.

Kayagaki, N., Warming, S., Lamkanfi, M., Vande Walle, L., Louie, S., Dong, J., Newton, K., Qu, Y., Liu, J., Heldens, S., et al. (2011). Non-canonical inflammasome activation targets caspase-11. Nature *479*, 117–121.

Kayagaki, N., Stowe, I.B., Lee, B.L., O'Rourke, K., Anderson, K., Warming, S., Cuellar, T., Haley, B., Roose-Girma, M., Phung, Q.T., et al. (2015). Caspase-11 cleaves gasdermin D for non-canonical inflammasome signalling. Nature *526*, 666–671.

Kim, Y., Zhou, P., Qian, L., Chuang, J.Z., Lee, J., Li, C., Iadecola, C., Nathan, C., and Ding, A. (2007). MyD88-5 links mitochondria, microtubules, and JNK3 in neurons and regulates neuronal survival. J. Exp. Med. *204*, 2063–2074.

Liu, X., Zhang, Z., Ruan, J., Pan, Y., Magupalli, V.G., Wu, H., and Lieberman, J. (2016). Inflammasome-activated gasdermin D causes pyroptosis by forming membrane pores. Nature *535*, 153–158.

Misawa, T., Takahama, M., Kozaki, T., Lee, H., Zou, J., Saitoh, T., and Akira, S. (2013). Microtubule-driven spatial arrangement of mitochondria promotes activation of the NLRP3 inflammasome. Nat. Immunol. *14*, 454–460.

Monteleone, M., Stanley, A.C., Chen, K.W., Brown, D.L., Bezbradica, J.S., von Pein, J.B., Holley, C.L., Boucher, D., Shakespear, M.R., Kapetanovic, R., et al. (2018). Interleukin-1β Maturation Triggers Its Relocation to the Plasma Membrane for Gasdermin-D-Dependent and -Independent Secretion. Cell Rep. *24*, 1425–1433.

Motani, K., Kushiyama, H., Imamura, R., Kinoshita, T., Nishiuchi, T., and Suda, T. (2011). Caspase-1 protein induces apoptosis-associated speck-like protein containing a caspase recruitment domain (ASC)-mediated necrosis independently of its catalytic activity. J. Biol. Chem. *286*, 33963–33972.

Mukherjee, P., Woods, T.A., Moore, R.A., and Peterson, K.E. (2013). Activation of the innate signaling molecule MAVS by bunyavirus infection upregulates the adaptor protein SARM1, leading to neuronal death. Immunity *38*, 705–716.

O'Neill, L.A., and Bowie, A.G. (2007). The family of five: TIR-domain-containing adaptors in Toll-like receptor signalling. Nat. Rev. Immunol. *7*, 353–364.

Osterloh, J.M., Yang, J., Rooney, T.M., Fox, A.N., Adalbert, R., Powell, E.H., Sheehan, A.E., Avery, M.A., Hackett, R., Logan, M.A., et al. (2012). dSarm/Sarm1 is required for activation of an injury-induced axon death pathway. Science *337*, 481–484.

Panneerselvam, P., Singh, L.P., Selvarajan, V., Chng, W.J., Ng, S.B., Tan, N.S., Ho, B., Chen, J., and Ding, J.L. (2013). T-cell death following immune activation is mediated by mitochondria-localized SARM. Cell Death Differ. *20*, 478–489.

Próchnicki, T., and Latz, E. (2017). Inflammasomes on the Crossroads of Innate Immune Recognition and Metabolic Control. Cell Metab. *26*, 71–93.

Rühl, S., Shkarina, K., Demarco, B., Heilig, R., Santos, J.C., and Broz, P. (2018). ESCRT-dependent membrane repair negatively regulates pyroptosis downstream of GSDMD activation. Science *362*, 956–960.

Sborgi, L., Rühl, S., Mulvihill, E., Pipercevic, J., Heilig, R., Stahlberg, H., Farady, C.J., Müller, D.J., Broz, P., and Hiller, S. (2016). GSDMD membrane pore formation constitutes the mechanism of pyroptotic cell death. EMBO J. *35*, 1766–1778.

Sester, D.P., Thygesen, S.J., Sagulenko, V., Vajjhala, P.R., Cridland, J.A., Vitak, N., Chen, K.W., Osborne, G.W., Schroder, K., and Stacey, K.J. (2015). A novel flow cytometric method to assess inflammasome formation. J. Immunol. *194*, 455–462.

Shi, J., Zhao, Y., Wang, K., Shi, X., Wang, Y., Huang, H., Zhuang, Y., Cai, T., Wang, F., and Shao, F. (2015). Cleavage of GSDMD by inflammatory caspases determines pyroptotic cell death. Nature *526*, 660–665.

Shi, H., Murray, A., and Beutler, B. (2016). Reconstruction of the Mouse Inflammasome System in HEK293T Cells. Bio Protoc. *6*, e1986.

Szretter, K.J., Samuel, M.A., Gilfillan, S., Fuchs, A., Colonna, M., and Diamond, M.S. (2009). The immune adaptor molecule SARM modulates tumor necrosis factor alpha production and microglia activation in the brainstem and restricts West Nile Virus pathogenesis. J. Virol. *83*, 9329–9338.

Waldhuber, A., Puthia, M., Wieser, A., Cirl, C., Dürr, S., Neumann-Pfeifer, S., Albrecht, S., Römmler, F., Müller, T., Zheng, Y., et al. (2016). Uropathogenic Escherichia coli strain CFT073 disrupts NLRP3 inflammasome activation. J. Clin. Invest. *126*, 2425–2436.

Wolf, A.J., Reyes, C.N., Liang, W., Becker, C., Shimada, K., Wheeler, M.L., Cho, H.C., Popescu, N.I., Coggeshall, K.M., Arditi, M., and Underhill, D.M. (2016). Hexokinase Is an Innate Immune Receptor for the Detection of Bacterial Peptidoglycan. Cell *166*, 624–636.

Yang, D., He, Y., Muñoz-Planillo, R., Liu, Q., and Núñez, G. (2015). Caspase-11 Requires the Pannexin-1 Channel and the Purinergic P2X7 Pore to Mediate Pyroptosis and Endotoxic Shock. Immunity *43*, 923–932.

Yu, J., Nagasu, H., Murakami, T., Hoang, H., Broderick, L., Hoffman, H.M., and Horng, T. (2014). Inflammasome activation leads to Caspase-1-dependent mitochondrial damage and block of mitophagy. Proc. Natl. Acad. Sci. USA *111*, 15514–15519.

Zanoni, I., Tan, Y., Di Gioia, M., Broggi, A., Ruan, J., Shi, J., Donado, C.A., Shao, F., Wu, H., Springstead, J.R., and Kagan, J.C. (2016). An endogenous caspase-11 ligand elicits interleukin-1 release from living dendritic cells. Science *352*, 1232–1236.

Zanoni, I., Tan, Y., Di Gioia, M., Springstead, J.R., and Kagan, J.C. (2017). By Capturing Inflammatory Lipids Released from Dying Cells, the Receptor CD14 Induces Inflammasome-Dependent Phagocyte Hyperactivation. Immunity *47*, 697–709.e3.

Zhang, Q., Zmasek, C.M., Cai, X., and Godzik, A. (2011). TIR domain-containing adaptor SARM is a late addition to the ongoing microbe-host dialog. Dev. Comp. Immunol. *35*, 461–468.

Zheng, Y., Humphry, M., Maguire, J.J., Bennett, M.R., and Clarke, M.C. (2013). Intracellular interleukin-1 receptor 2 binding prevents cleavage and activity of interleukin-1α, controlling necrosis-induced sterile inflammation. Immunity *38*, 285–295.

Zhong, Z., Liang, S., Sanchez-Lopez, E., He, F., Shalapour, S., Lin, X.J., Wong, J., Ding, S., Seki, E., Schnabl, B., et al. (2018). New mitochondrial DNA synthesis enables NLRP3 inflammasome activation. Nature *560*, 198–203.

STAR★METHODS

KEY RESOURCES TABLE

REAGENT or RESOURCE	SOURCE	IDENTIFIER
Antibodies		
ASC	Santa Cruz	sc-22514R; RRID: AB_2174874
Caspase 1	Adipogen	AG-20B-0042; RRID: AB_2490248
NLRP3	Adipogen	AG-20B-0014; RRID: AB_2490202
MyC	Sigma-Aldrich	M5546; RRID: AB_260581
Flag	Sigma-Aldrich	F-3165; RRID: AB_259529
HA	Biolegend	901515; RRID: AB_2565334
IL-1β	R&D	AF-401-NA; RRID: AB_416684
β actin	Sigma-Aldrich	A5316; RRID: AB_476743
GAPDH	Cell Signalling	2118; RRID: AB_561053
Acetylated Tubulin	Sigma-Aldrich	T6793; RRID: AB_477585
Caspase 11	Sigma-Aldrich	C1354; RRID: AB_258736
Gasdermin D	Sigma-Aldrich	G7422; RRID: AB_1850381
Histone H3	Upstate technologies	05-499; RRID: AB_309763
VDAC	Abcam	ab15895; RRID: AB_2214787
α-tubulin	Sigma-Aldrich	T5168; RRID: AB_477579
Alexa Fluor 647	Invitrogen Molecular Probes	A21245; RRID: AB_2535813
Alexa Fluor 488	Invitrogen Molecular Probes	A11029; RRID: AB_138404
Alexa Fluor 488 conjugated anti-Flag antibody	Cell signalling	5407S; RRID: AB_1950473
Chemicals, Peptides, and Recombinant Proteins		
LPS	ENZO	581-010-L002
Pam_3CSK_4	Invivogen	tlrl-pms
Nigericin	Invivogen	tlrl-nig
Peptidoglycan	Sigma-Aldrich	77140
MCC950	Luke O'Neill Laboratory	N/A
YVAD	Sigma-Aldrich	SML0429
disuccinimidyl suberate (DSS)	Fisher Scientific	11831255
TMRM	Sigma-Aldrich	T5428
Mitotracker RED CMXRos	Invitrogen Molecular probes	M7512
Mitotracker green	Invitrogen Molecular probes	M7514
Phalloidin-FITC	Sigma-Aldrich	P5282
Fc block	BD Biosciences	553141
DAPI	Invitrogen Molecular probes	D1306
MOWIOL (4.88)	Calbiochem	475904
poly-L-lysine	Sigma-Aldrich	P4707
Streptavidin conjugated 488	Invitrogen Molecular probes	S11223
Genejuice	Merck Millipore	70967-4
Lipofectamine 2000	Invitrogen	11668019
OptiMem	ThermoFisher	11058021
Critical Commercial Assays		
CytoTox 96 Non-Radioactive Cytotoxicity Assay (LHD assay)	Promega	G1780
Murine IL-1β ELISA	R&D	SMLB00C
Murine IL-1β ELISA	Biolegend	432601

(*Continued on next page*)

Continued

REAGENT or RESOURCE	SOURCE	IDENTIFIER
Murine IL-1α ELISA	Biolegend	433401
Murine IL-18 ELISA	MBL	7625
Murine TNF-α ELISA	R&D	SMTA00B
Murine IFNβ ELISA (Capture antibody)	Santa Cruz	SC-57201
Murine IFNβ ELISA (Detection antibody)	PBL InterferonSource	32400-1
Murine IFNβ ELISA (Standard)	PBL InterferonSource	12400-1
High Pure RNA Isolation Kit	Roche	11828665001
Moloney murine leukemia virus reverse transcriptase	Promega	M1701
Neon Transfection System	Invitrogen	MPK5000S
Neon Transfection System 100 μL Kit	Invitrogen	MPK10096
Experimental Models: Cell Lines		
Wild-type immortalized BMDMs	Kate Fitzgerald Laboratory	N/A
SARM$^{-/-}$ immortalized BMDMs	Prof. Kate Fitzgerald Laboratory	N/A
HEK 293T cells	Andrew Bowie Laboratory	N/A
Experimental Models: Organisms/Strains		
C57BL/6 mice	Trinity Biomedical Sciences Institute (TBSI), Trinity College Dublin (TCD)	N/A
Sarm$^{-/-}$ mice (B6.129X1-*Sarm1*^{tm1Aidi}/J)	The Jackson Laboratory, bred in TBSI, TCD	JAX stock #018069; PMID: 24711619; PMID: 17724133
Oligonucleotides		
NLRP3 forward primer for qPCR	Integrated DNA Technologies	CCACATCTGATTGTGTTAATGGCT
NLRP3 reverse primer for qPCR	Integrated DNA Technologies	GGGCTTAGGTCCACACAGAA
Pycard (which encodes ASC) forward primer for qPCR	Integrated DNA Technologies	ACTGTGCTTAGAGACATGGGC
Pycard (which encodes ASC) reverse primer for qPCR	Integrated DNA Technologies	TGGTCCACAAAGTGTCCTGTT
β-actin forward primer for qPCR	Integrated DNA Technologies	TCCAGCCTTCCTTCTTGGGT
β-actin reverse primer for qPCR	Integrated DNA Technologies	GCACTGTGTTGG CATAGAGGTC
Recombinant DNA		
Human SARM Flag-tagged	This paper	N/A
Human NLRP3 Myc-tagged	Dan Kastner Laboratory	N/A
Human ASC HA-tagged (pCI-ASC-HA)	Luke O'Neill Laboratory	RRID: Addgene_41553
Mouse SARM in pMSCV-NEO	PMID: 24711619	N/A
Mouse SAMTIR in pMSCV-PIG	This paper	N/A
Mouse TIR in pMSCV-PIG	This paper	N/A
Mouse SARM in pdINotInPkMCSR	This paper; PMID: 23431397	N/A
pMD2.G (VSV-G)	PMID: 23431397	RRID: Addgene_12259
pCMVR8.91 (Gag/Pol, Tat and Rev)	PMID: 23431397	N/A
pcDNA3-N-Flag-NLRP3	Luke O'Neill Laboratory; PMID: 28516117	RRID: Addgene_75127
pcDNA3-N-Flag-ASC1	Luke O'Neill Laboratory; PMID: 28516117	RRID: Addgene_75134
pcDNA3-N-Flag-Caspase-1	Luke O'Neill Laboratory; PMID: 28516117	RRID: Addgene_75128
pCMV-pro-IL1β-C-Flag	Luke O'Neill Laboratory; PMID: 28516117	RRID: Addgene_75128
Software and Algorithms		
ImageJ	NIH	https://imagej.nih.gov/
FlowJo Software	FlowJo	N/A
GraphPad Prism	GraphPad Software, Inc	N/A

CONTACT FOR REAGENT AND RESOURCE SHARING

Further information and requests for resources and reagents should be directed to and will be fulfilled by the Lead Contact, Andrew G. Bowie (agbowie@tcd.ie).

EXPERIMENTAL MODEL AND SUBJECT DETAILS

Mice

C57BL/6 mice lacking *Sarm1* were described previously (Gürtler et al., 2014; Kim et al., 2007). The mice were bred and housed at the Trinity Biomedical Sciences Institute, Trinity College Dublin. All mice experiments were performed in compliance with the Irish Health Products Regulatory Authority and approved by Trinity College Dublin's BioResources ethical review board. Primary BMDM and iBMDM were generated from wild type and *Sarm1*$^{-/-}$ mice as previously described (Gürtler et al., 2014). Immortalized WT and *Sarm1*$^{-/-}$ BMDMs were generated with J2 recombinant retrovirus carrying v-myc and v-raf oncogenes.

Cell culture

BMDMs were mycoplasma-free and were cultured in DMEM, supplemented with 10% FCS (v/v) and 10 μg/mL ciprofloxacin and kept at 37°C with 5% CO_2. Primary and immortalized WT and *Sarm1*$^{-/-}$ BMDMs were grown in DMEM plus GlutaMAX (Life Technologies), containing 10% FCS and 10 μg/mL ciprofloxacin. Primary BMDMs from femurs were supplemented with 20% L929 supernatant as a source of M-CSF (Gürtler et al., 2014). On day 7, the BMDMs were seeded for experiments in DMEM containing 15%–20% (v/v) L929 supernatant. HEK293T cells were cultured in DMEM, supplemented with 10% FCS (v/v) and 10 μg/mL ciprofloxacin and kept at 37°C with 5% CO_2.

Retroviral transduction of iBMDM

Retroviral transduction of iBMDM was used to express SARM and SARM truncations in wild type and *Sarm1*$^{-/-}$ cells. SARM was subcloned from pGW1-SARM1 with a C-terminal Flag-tag attached into the retroviral expression vector pMSCV-neo (Gürtler et al., 2014). Retroviral particles were produced in HEK293T cells: cells were seeded at 2x10^5 cells/mL in 10-cm dishes and transfected 24 h later with 3 μg pMSCV empty vector control or pMSCV-SARM-FLAG, together with 1 μg VSV-G and 1 μg Gag-Pol plasmids using 15 μL GeneJuice. Medium was replaced 8 h later and retroviral supernatants were harvested 48 and 72 h after transfection, centrifuged, and filtered through a 0.45 mm filter. WT iBMDM cells were seeded at 3x10^5 cells/mL in six-well plates and spinoculated the next day with viral supernatant containing 8 μg/mL polybrene at 2000 *g* for 1 h. Spinoculation was repeated 24 h later, and expression of exogenous protein was confirmed by Flag immunoblot. WT iBMDMs stably expressing SARM were selected by the addition of G418 at 1 mg/mL. The SARM truncations along with a C-terminal Flag tag was cloned into the XhoI and EcoRI restriction sites of the pMSCV_PIG vector using standard PCR and cloning techniques and introduced into iBMDMs as above.

Generation of *Sarm1*$^{-/-}$ iBMDMs stably expressing SARM

Flag-tagged murine SARM was cloned into the pdINotInPkMCSR lentiviral expression vector and transfected along with VSV G protein (pMD-G) and Gag/Pol, Tat and Rev proteins (pCMVR8.91) into HEK 293T cells, according to the method by Chinnakannan et al (2013) (Chinnakannan et al., 2013). The resulting viruses were introduced into *Sarm1*$^{-/-}$ iBMDMs by spinoculation. 48 h later puromycin at a concentration of 5 μg/mL was added to the *Sarm1*$^{-/-}$ iBMDMs to select the SARM expressing cells.

Induction of LPS-induced sepsis

Prior to induction of LPS-induced sepsis (Hams et al., 2011), temperature transponder chips (Bio Medic Data Systems; IPTT-300) were implanted s.c. into the mice, to allow for non-invasive temperature monitoring throughout. Shock was induced in mice via i.p. injection of ultrapure LPS extracted from Escherichia coli (Invivogen) at a dose of 10 mg/kg. Animals were scored at hourly intervals using the following criteria: score 0 = no symptoms; score 1 = piloerection, huddling; score 2 = piloerection, huddling, diarrhoea; score 3 = lack of interest in surroundings, severe diarrhoea; score 4 = decreased movement, listless appearance; and score 5 = loss of self-righting reflex. When mice reached a score of 5, they were humanely euthanized. For serum cytokine analysis groups of age-matched male C57 and *Sarm1*$^{-/-}$ mice were injected i.p. with 10 mg/kg UP-LPS. After 3 h mice were sacrificed and blood was collected via cardiac puncture for measurement of serum cytokines.

METHOD DETAILS

Inflammasome activation and analysis

For inflammasome activation, cells were primed with LPS (Enzo, 200 ng/mL) or Pam_3CSK_4 (InvivoGen, 1 μg/mL) for 4 h and treated with nigericin (InvivoGen, 10 μM) for 1 h, 3 h or 20 h or with peptidoglycan (PGN, Sigma-Aldrich, 50 μg/mL) for 6 h or 20 h. In experiments where MCC950 (a gift from Luke O'Neill, Trinity College Dublin, Ireland) and YVAD (Sigma-Aldrich) were used, these were added just prior to the addition of nigericin. To evaluate caspase-11 dependent responses, iBMDMs were first primed with LPS (200 ng/mL) for 4 h and 1 million cells were then electroporated with 2 μg LPS for 16 h. The electroporation was performed using the NEON Transfection System (Life Technologies), where 1400 volts, 10 pulse width and 2 pulses were chosen. Pyroptosis was

assessed by LDH release (LDH Cytotoxicity Assay Kit (Thermo Scientific) or the CytoTox 96 Non-Radioactive Cytotoxicity Assay (Promega)), caspase-1 activation and IL-1β processing by immunoblot (see below), and IL-1β, IL-1α and IL-18 release by ELISA (see below).

Immunoblotting

10 million iBMDMs were primed with LPS for 4 h and treated with nigericin for 1 h. The cells were lysed in Laemmli sample buffer and stored at −20°C until analysis, or immediately sonicated, boiled, and subjected to SDS-PAGE. Proteins in the supernatants were precipitated using strataclean resin (Agilent) using 10 μL resin/mL of supernatant and rotated at 4°C overnight. Supernatants were removed and, after Laemmli sample buffer was added, boiled and subjected to SDS-PAGE and immunoblotting. PVDF membranes were probed with antibodies for either IL-1β (Cat# AF-401-NA, R&D) or caspase-1 (Cat# AG-20B-0042**,** Adipogen). Other antibodies used were, NLRP3 (Cat# AG-20B-0014, Adipogen), ASC (Cat# sc-22514R, Santa Cruz), β-actin (Cat# A5316, Sigma), GAPDH (Cat# 2118, Cell Signaling), Flag (Cat# F-3165, Sigma). Acetylated Tubulin (Cat# T6793, Sigma), Caspase-11 (Cat # C1354, Sigma), Gasdermin D (Cat# G7422, Sigma).

RNA analysis by quantitative RT-PCR

For iBMDMs, total RNA was extracted from cells using the High Pure RNA Isolation Kit (Roche) and reverse transcribed with random hexamers (IDT) using Moloney murine leukemia virus reverse transcriptase (Promega) according to the manufacturer's instructions. mRNA was quantified with SYBR Green using primer pairs targeting *nlrp3* (Forward 5′-CCACATCTGA TTGTGTTAATGGCT-3′, Reverse 5′-GGGCTTAGGTCCACACAGAA-3′), *pycard* (which encodes ASC) (Forward 5′-ACTGTGCTTAGAGACATGGGC-3′, Reverse 5′-TGGTCCACAAAGTGTCCTGTT-3′) and β-actin (Forward 5′-TCCAGCCTTCCTTCTTGGGT-3′, Reverse 5′-GCACTGTGTTGG CATAGAGGTC-3′). Relative mRNA expression was calculated using the comparative C_T method, normalizing the gene of interest to the housekeeping gene β-actin, analyzing the data as fold induction compared to that of the control sample.

Enzyme-linked immunosorbent assay

Quantification of secreted murine IL-1α and IL-1β was performed using ELISA kits from Biolegend, while murine TNFα was measured using ELISA kits from R&D. Murine IL-18 was detected using an ELISA kit from MBL. Detection of mouse IFNβ production by ELISA was performed using a monoclonal rat anti-mouse IFNβ antibody as a capture antibody (Santa Cruz Cat# SC-57201). A polyclonal rabbit anti-mouse IFNβ antibody (Cat# 32400-1, PBL InterferonSource) was used as a detection antibody, while a HRP-conjugated anti-rabbit IgG conjugated antibody (Cat# RABHRP1, Sigma) was used for TMB substrate (BD) development. The murine IFNβ standard was from PBL InterferonSource (Cat# 12400-1).

ASC oligomerization assay

15 million iBMDMs were primed with LPS for 4 h and then treated with nigericin for 1 h. The cells were collected and lysed in lysis buffer (50mM Hepes, 100 mM NaCl, 1 mM EDTA, 10% glycerol and 1% NP40 and the inhibitors 1% aprotinin, 1 mM PMSF, and 1 mM sodium orthovanadate). The cell lysates were centrifuged at 14000 *g* for 5 min at 4°C and supernatants collected in a fresh tube. Laemmli sample buffer was added to 10% of the supernatant, which was boiled and subjected to SDS-PAGE and immunoblotting. The PVDF membranes were probed for ASC or β-actin. Cell pellets were cross-linked in a 5 mM solution of disuccinimidyl suberate (DSS) in PBS and rotated at room temp for 45 min. Laemmli sample buffer was then added to the cross-linked pellets, which were boiled and subjected to SDS-PAGE. Immunoblot was performed with antibodies for ASC or histone H3 (Cat# 05-499, Upstate technologies).

Visualization of ASC speck formation using confocal microscopy

Cells were seeded on coverslips and stimulated as above to activate the NLRP3 inflammasome. The cells were fixed in 4% paraformaldehyde and permeabilized in 0.5% Triton X-100. The coverslips were blocked using 5% BSA in a solution of 0.05% TWEEN 20 in PBS. The anti-ASC antibody (Cat# sc-22514R, Santa Cruz) was added at a concentration of 2 μg/mL and incubated overnight at 4°C. Alexa Fluor 647 secondary antibody (1:2000) was used for 1 h at room temp. To stain the actin cytoskeleton phalloidin-FITC (Sigma) was used at 1:1000 for 1 h at room temp. The coverslips were mounted in Mowiol 4-88 (Calbiochem) containing DAPI (4,6-diamidino-2-phenylindole, 1 μg/mL). An Olympus FV1000 scanning confocal microscope was used to collect images.

Analysis of ASC speck formation by flow cytometry

A protocol adapted from Sester et al. (2015) was employed. Cells were harvested with ice-cold PBS, centrifuged at 1,000 *g* for 5 min and resuspended in 1 mL ice-cold PBS. Samples were then fixed by the dropwise addition of 4 mL ice-cold molecular grade ethanol while vortexing. After 15 min cells were pelleted by centrifugation at 600 *g* for 10 min, supernatants gently removed and pellets resuspended in 250 μL ASC speck buffer (ASB, PBS/0.1% sodium azide, 0.1% BSA, 1.5% FCS) containing 1 μL Fc block (BD Biosciences) for 20 min. 50 μL ASB containing 0.2 μl anti-ASC (Cat# sc-22514R, Santa Cruz) was added and left for 90 min. 1 mL ASB was added and pellets were resuspended in 50 μL ASB containing 0.1 μl Alexa Fluor 488 goat anti-rabbit IgG (H+L) (Molecular Probes). After 45 min, 1 mL ASB was added and pellets were resuspended in 500 μL ASB. Samples were processed on a BD FACSCanto and analyzed using FloJo.

Visualization of SARM localization after inflammasome activation

Flag-tagged SARM (Flag-SARM) expressing iBMDMs were treated, fixed, and permeabilized as above. To stain mitochondria, 30 min before harvesting MitoTracker Red was added at a concentration of 250 nM. Flag-SARM was detected using the Flag antibody (Sigma) at a dilution of 1:500 overnight at 4°C, and then anti-mouse Alexa Fluor 488 secondary antibody (1:2000) treatment for 1 h at room temperature. Coverslips were mounted as above and images were collected using a Leica SP8 scanning confocal microscope.

Analysis of SARM clustering by confocal microscopy

Sarm1$^{-/-}$ iBMDMs stably expressing SARM were seeded onto coverslips and primed with 200 ng/mL of LPS for 4 h and either treated with 10 μM Nigericin for 1hr or 50 μg/mL peptidoglycan for 6 h. 30 min before harvesting mitotracker red was added at a concentration of 250 nM. The cells were fixed using 4% formaldehyde and permeabilized using 0.5% Triton-X-100. An Alexa Fluor 488 conjugated anti-Flag antibody (Cell Signaling Cat# 5407S) was added at a concentration of 1:500 in 5% BSA in 0.05% PBS-Tween and incubated overnight. The coverslips were then washed using PBS and mounted in Mowiol containing DAPI. The slides were then analysed using a Leica confocal microscope.

Isolation of mitochondria

40 million *Sarm1*$^{-/-}$ iBMDMs stably expressing Flag-SARM or EV were seeded per condition and left to adhere overnight. Cells were primed with 200 ng/mL of LPS or not for 4 h and stimulated with 10 μM nigericin or not for 1 h. Cells were scraped, washed twice in PBS and re-suspended in 1 mL buffer containing 320 mM sucrose, 10 mM TRIS, 1 mM EDTA and protease inhibitors. The samples were briefly sonicated and the lysates were centrifuged at 700 *g* for 10 min at 4° C. The resulting supernatants were removed and centrifuged at 3,000 *g* for 15 min at 4°C to isolate the heavy mitochondrial fraction. The isolated mitochondrial pellets were washed 6 times with PBS. The remaining supernatants were spun at 12,000 *g* for 20 min to remove light mitochondria, peroxisomes, and lysosomes, and the cytosolic fractions were harvested. Laemmli sample buffer containing DTT was added to the mitochondrial and cytosolic fractions. The samples were sonicated, boiled, and resolved on SDS-PAGE. Immunoblotting was performed for VDAC (Abcam , # ab15895) as a marker for mitochondria, for α-tubulin (Sigma-Aldrich, Cat# T5168) as a marker for the cytosol, and for Flag-SARM.

Visualization of IL-1β secretion from single cells

This method was adapted from Cullen et al. (2015). Mouse IL-1β capture antibody (BioLegend) at 200X concentration was added to poly-L-lysine (Sigma) coated coverslips (coverslips were coated overnight). iBMDMs seeded overnight on coverslips were stimulated with 200 ng/mL LPS for 4 h followed by 1 h of 10 uM nigericin treatment. 30 min before harvesting Mitotracker Red was added at a concentration of 250 nM. Mouse IL-1β detection antibody (BioLegend) was added at a 200X concentration to the cells on the coverslips for 2 h at room temperature. Streptavidin conjugated 488 (Molecular Probes) was added at a dilution of 1:2000 in PBS for 1 h at room temperature. Following gently washing with PBS, the coverslips were fixed in 4% paraformaldehyde and mounted in Mowiol 4-88 containing DAPI. Coverslips were stored at 4°C until microscopy analysis. Images were collected using a Leica SP8 scanning confocal microscope.

Co-immunoprecipitation of proteins

For endogenous co-immunoprecipitation of ASC and NLRP3, 15 million iBMDMs were collected and lysed in lysis buffer containing: 50 mM Hepes, 100 mM NaCl, 1 mM EDTA, 10% glycerol and 1% NP40 and the inhibitors 1% aprotinin, 1 mM PMSF, and 1 mM sodium orthovanadate. The cell lysates were centrifuged at 14,000 *g* for 5 min at 4°C. Endogenous ASC from iBMDMs was immunoprecipitated from the cell lysates overnight at 4°C and samples immunoblotted for NLRP3 and ASC. For co-immunoprecipitation of ectopically expressed proteins, human SARM was cloned from the p-UNO vector (Invitrogen) into the pEF-Bos vector expressing a C-terminal Flag tag. Human myc-NLRP3 was a gift from Prof. Dan Kastner (National Institute of Arthritis and Musculoskeletal and Skin Diseases, Bethesda, Maryland). HEK293T cells were transfected with human Flag-SARM and Myc-NLRP3 or with pCI HA-ASC. 48 h later the cells were lysed (as above) and immunoprecipitated using antibodies against Flag and immunoblotted as indicated.

Reconstitution of NLRP3 inflammasome in HEK293T cells

Reconstruction of the mouse inflammasome assay was adapted from the method described previously (Shi et al., 2016). Briefly, HEK293T cells were seeded at 2x10^5 cells/well in 24-well plates and incubated overnight. The cells were transfected with plasmids with 50 ng mouse pro-IL-β-FLAG plasmid, 10 ng mouse pro-Caspase-1-FLAG plasmid, 1 ng mouse ASC-FLAG plasmid, 50 ng mouse NLRP3 plasmid and 200 ng pdlNotInPkMCSR SARM-FLAG vector or pdlNotInPkMCSR empty vector control using 1.5 μL Lipofectamine 2000. Medium was replaced 24 h after transfection and supernatants were collected 16 h after media change. Quantification of secreted murine IL-1β was performed using ELISA.

Analysis of mitochondrial depolarization

All steps were carried out on ice except where noted. WT iBMDMs or *Sarm1*$^{-/-}$ iBMDMs were seeded at 5 x 10^5 cells/ml in 24-well plates and left overnight to adhere. After cell stimulations the cell monolayer was disrupted by gently pipetting the supernatant up and

down. The supernatant was then transferred into flow cytometry tubes. 500 μL-1 mL ice-cold PBS was then added to each well for one min. The PBS was then pipetted up and down to dislodge the remaining adhered cells and transferred to the corresponding flow cytometry tube. Cells were centrifuged at 1,000 *g* for 5 min and washed three times with PBS. A staining solution of DMEM containing a final concentration of 25 μM tetramethylrhodamine (TMRM) was prewarmed to 37°C. Cell pellets were resuspended in 1 mL of the staining solution, covered in tin foil and incubated for 30 min at 37°C. Samples were then centrifuged and washed three times with PBS/1 % BSA. Samples were processed on a BD LSRFortessa ((561nm) 610/20nm channel) and analysed with FlowJo.

To compare MDP in nigericin- and PGN-treated cells, iBMDMs were primed with 200 ng/mL of LPS for 4 h and either treated with 10 μM nigericin for 1 h or 50 μg/mL peptidoglycan for 6 h. The cell monolayer was disrupted with PBS and transferred into flow cytometry tubes. Cells were centrifuged at 1,000 *g* for 5 min and washed once with PBS. A staining solution of 100 nM TMRM and 100 nM MitoTracker Green (MTG) in pre-warmed serum free media was used to re-suspend cell pellets. Samples were incubated at 37°C for 30 mins in the dark. Cells were centrifuged, washed three times in PBS and resuspended in 200 μl PBS/2 % BSA. 50 μM FCCP was added to sample just before analysing. Cells were acquired using LSRFortessa flow cytometer using (562 nm) 610/20 nm channel for TMRM and (488 nm) 530/30 nm channel for MTG. The data were analysed using FlowJo software. For gating strategy, all cells were gated excluding debris (bottom left corner). Cells that maintained MTG but lost TMRM from this population (TMRM on y-axis, MTG on x-axis) were considered to have depolarized mitochondria.

QUANTIFICATION AND STATISTICAL ANALYSIS

Data were analyzed using unpaired Student's t test or Spearman rank correlation as indicated in legends. Data are representative of at least an n = 3 (3 independent experiments) and data are presented as mean ± standard deviation or standard error of the mean as indicated in the figure legends. GraphPad Prism 8 was used to calculate p values, and significance is depicted with asterisks on graphs as follows: *$p < 0.05$, **$p < 0.01$, ***$p < 0.001$, ****$p < 0.0001$.